Numerical Study of an Observed Orogenic Mesoscale Convective System. Part 1: Simulated Genesis and Comparison with Observations

GREGORY J. TRIPOLI* AND WILLIAM R. COTTON

Colorado State University, Department of Atmospheric Science, Fort Collins, Colorado

(Manuscript received 10 October 1987, in final form 17 June 1988)

ABSTRACT

The interaction of topographically induced thermally and mechanically driven diurnal flow regimes in the lee of the Rockies is shown to lead to the growth of a mesoscale convective system (MCS). An orogenic MCS observed during the 1977 combined South Park Area Cumulus Experiment and High Plains Experiment is numerically simulated with a two-dimensional nonhydrostatic cloud model covering spatial scales of 1000 km. In this numerical investigation, mesoγ-, mesoβ- and mesoα-scales of motion are represented simultaneously. As a result, interesting features of cloud–mesoscale interaction are predicted that cannot be represented in cloud parameterization frameworks. Based on the results of this simulation, a six-stage conceptual model of orogenic development is given.

1. Introduction

Summertime convective rainfall in the midwestern United States occurs primarily at night despite higher daytime conditional instability. Studies of rainfall climatology by Kincer (1916), Crow (1969) and Wallace (1975) demonstrate that the most frequent time of summer convective precipitation occurrence moves gradually from early in the afternoon over the Rockies to the middle of the night over the Central Great Plains. Although it was first argued that long-wave radiation emission led to the nocturnal rains (Hann 1926; Hewson 1937), the discovery of the low-level nocturnal southerly jet by Means (1944, 1952) supplied convincing evidence that the nocturnal rains were dependent on CAPE (convective available potential energy) supplied from this nocturnal flow regime.

The relationship between convection over the Rockies and that over the plains remained unexplained until later when two schools of thought developed. In the first school were those who believed that convection across the region developed in situ from topographically induced local flow deformations. Explanations ranged from the influence of developing nocturnal slope flows in opposition to lingering daytime upslope flow (Bleeker and Andre 1951) to the influence of mountain-wave patterns (Dirks et al. 1967) and multicell slope circulations (Dirks 1969).

The other school argued that the increasingly later diurnal rain maxima with distance east of the Rockies resulted from a systematic progression of organized convection. Bonner (1963) first presented observational evidence to this effect and was followed by Wetzel (1973) who presented a compilation of 2 years of radar data establishing the link in eastern Colorado. Later, Phillip (1979) used satellite observations from the summers of 1976 and 1977 to show that the eastward progression of mountain convection seemed to occur on average about 15% of the days. More recently, Klitch et al. (1985) again found the diurnal eastward progression of convection from the Colorado Rockies in the satellite observations of the 1982 summer. They further observed a tendency for convection to favor the Palmer Lake Divide, an east–west oriented ridge on the western High Plains through central Colorado.

In the past decade, satellite observationalists have also paid considerable attention to the cloud systems producing the nocturnal rains over the Great Plains. Maddox (1980) defined a frequently observed circular satellite signature to be associated with the summertime nocturnal rains, which he called a Mesoscale Convective Complex (MCC). After compositing satellite and conventional observations of these systems for a two-year period, Maddox was able to demonstrate that a favorable region for genesis occurred over the Rocky Mountains, supporting the idea that the nocturnal convection is often orogenic (genesis under orographic influences).

The 1977 combined Colorado State University South Park Area Cumulus Experiment (SPACE) and High Plains Experiment (HiPLEX) was designed, in

* Current affiliation: University of Wisconsin, Dept. of Meteorology, Madison, WI 53715.

Corresponding author address: Dr William R. Cotton, Dept. of Atmospheric Sciences, Colorado State University, Fort Collins, CO 80523.

© 1989 American Meteorological Society

part, to investigate the linkage between Rocky Mountain and High Plains convection. The observational studies of Cotton et al. (1983, hereafter referred to as CGWM), Wetzel et al. (1983) and McAnelly and Cotton (1986) based on data collected during that experiment seemed to confirm the orogenic nature of some nocturnal convection over the Great Plains.

In a study of all MCCs in the Central United States over a 2-year period, Maddox (1981) determined that almost half of the cases were orogenic. More recently, in a similar study, Lin (1986) indicated that about 32 of 132 MCCs were orogenic.

The idea that the nocturnal rain maximum are induced by convection organized in some way and propagating as a weather system instead of developing in situ seems evident in light of these more recent investigations. However, many questions are left unanswered. Maddox (1981) defined the MCC by its infrared satellite signature; such a definition is ultimately unsatisfactory because it says nothing about the dynamics. The composite studies of Maddox (1983) and Lin (1986) suggest that these systems contain a significant mesoα-scale circulation between 90 and 20 kPa centered about a warm core. In Lin's composite MCC, anticyclonic relative vorticity of 2–5 ($\times 10^{-5}$ s^{-1}) was found within the anvil at 20 kPa, while cyclonic relative vorticity of 0–0.5 ($\times 10^{-5}$ s^{-1}) was found near 70 kPa. In addition, he finds mean vertical motion between those levels increasing to the mature phase and persisting for some time after the convection has weakened. These findings are consistent with the hypothesis that there is an important semigeostrophic component to these systems. In effect, the persistent semigeostrophic circulation is spun up by the convective heating and thereafter acts as a dynamic "flywheel" (Emanuel 1983) by supporting a persistent deep vertical motion in response to the ageostrophic portion of the circulation.

As with most other weather systems, the solution to the development question is perhaps the most elusive. At the mature phase, composites suggest the usual simultaneous occurrence of an upper-level disturbance situated near the MCC. However, the composite situation prior to formation is much less disturbed, and some individual case studies reveal no obvious preexisting upper-level disturbance (CGWM). This suggests that although many of these convective systems arise in the vicinity of a 50 kPa short-wave disturbance, it is not a necessary condition. In fact, their diurnal nature indicates that an existing disturbance only enhances the local conditions for MCC development. Important local triggers for MCS development may include thermally driven solenoidal circulations associated with sloped terrain, land–water boundaries, dryline boundaries, airmass boundaries, soil moisture boundaries and others.

To increase our skill in predicting summertime rainfall in the lee of the Rockies, it is necessary to reach a greater understanding of the MCC in both its structure and origins. The high-quality observational network established for the SPACE 1977 experiment provided an unprecedented detailed look at the development of several orogenic MCCs. The 4 August 1977 case was particularly robust because it seemed to be free of a high degree of external forcing and because of the high-quality of observations. The observational studies of this case described by CGWM followed the convection through several phases of development from mountain cumulus congestus to a classic nocturnal MCC over Kansas. The observations seemed to support the hypothesis that the system was self-exciting but failed to identify the dynamical mechanism.

In this series of two papers, a nonhydrostatic primitive equation model of the observed development scenario is employed as a tool for investigating the nature of orogenic development and studying the salient dynamics. The goal, in this study, will be to support the hypothesis that the orogenic development was, indeed, the major contributing factor to the observed MCS genesis and to propose a realistic scenario of how it might happen. Section 2 will briefly review the observational results of CGWM, Wetzel et al. (1983) and McAnelly and Cotton (1986) for this case, with new emphasis on features the model has elucidated as being important. Section 3 will describe the experimental design, including the numerical model physics, computation procedure, initialization and approach. Section 4 will describe the results of the numerical integration and compare them with observations. Finally, section 5 will summarize the results in the context of the original orogenic hypothesis. In Tripoli and Cotton (1988, hereafter referred to as Part 2), the dynamics involved throughout the system evolution will be explored, leading toward a conceptual model of orogenesis of MCCs.

2. The 4 August 1977 case study

The synoptic situation in and around Colorado on the morning of 4 August 1977 was only weakly disturbed. The 50 kPa (Fig. 3 of CGWM) analysis featured a long-wave trough centered over the Hudson Bay with an elongated subtropical high to the south, producing a nearly zonal flow from western Colorado to the central Mississippi valley. Cotton et al. (1983) note that this more zonal pattern formed over several days prior to the event and persisted for some time after. With the formation of this flow regime, an "episode" of diurnal MCC formation occurred, lasting a period of 8 days (Wetzel et al. 1983).

A zonal cross section analyzed for the morning of 4 August is displayed in Fig. 6 of CGWM. The movement of deep moisture from the west into Colorado was noted. This is associated with the eastward extension of the Southwest Monsoon (Hales 1972). Some investigators have linked the episodic development of orogenic mesoscale convective systems to the move-

ment of such monsoon moisture into western Colorado (Culverwell 1982; Wetzel et al. 1983).

At the surface, a weak east–west oriented cold front was situated on the north slope of the Cheyenne ridge (east–west oriented ridge of elevated topography along the Colorado and Wyoming border). By afternoon, the cold front advanced southward to the Palmer Lake Divide (east–west oriented ridge of elevated topography running through central Colorado 50 km south of Denver). This left a strong surface moisture gradient from southeastern to northeastern Colorado. At 1400 MST, CGWM depict surface mixing ratios of water vapor decreasing from 12 g kg^{-1} in Pueblo, Colorado, to 9 g kg^{-1} in Denver. At the same time, a stronger cold front advanced into Wyoming from the northwest during the day.

Both fronts were linked to 50 kPa short-wave disturbances, although the weaker front through Colorado was barely detectable. It was hypothesized that its major role in the development of mesoscale convection was the enhancement of low-level convergence on the High Plains. Moreover, because of its shallow depth, it effectively decoupled the surface from the active convection north of Denver. Afternoon surface observations combined with radar depictions suggested that convection became increasingly weak with distance north of Denver, apparently surviving on moisture advected over the front from the south. In fact, over Denver the surface air possessed essentially no CAPE during the afternoon and so the convection occurring could not be explained without considering the flow of moisture from the south.

Soundings taken at 0500 MST (1200 UTC) at six stations across the observation network are displayed in Fig. 1. In all cases east of the Continental Divide (all stations except Grand Junction), the atmosphere would be conditionally unstable following afternoon heating. These soundings do not depict the cool air to the north, which advected over Denver in the afternoon. Very high midlevel moisture moving into the area from the west at 50–70 kPa, more evident in Fig. 6 of CGWM, is beginning to appear at Grand Junction. This moisture will be especially important to mountain convection over South Park, where the daytime boundary-layer will strongly warm the 50–70 kPa layer. Over the plains stations from Denver eastward, the effect of the nocturnal inversion can be seen. Generally weak northwesterly flow is found in the lowest 2 km over the plains locations west of Topeka. The low-level winds reflect the nocturnal downslope wind regime. Note also the high moisture content over Topeka, Kansas, which reflects the lingering effects of an MCC from the previous night.

As reported by CGWM, the development of convection occurred in three stages. The first stage was characterized by the growth of the mountain boundary-layer over South Park. At sunrise, small-scale slope flows beneath the nocturnal inversion rapidly developed, followed by a larger-scale, more moist, cool valley wind 2 hours later. By 0900 MST, deep convection began over the mountain peaks and moved into South Park by 1100 MST. Cotton et al. (1983) report that observations of deep convection were coincident with the development of conditional instability from surface warming and moistening. Moistening was attributed to the advection from the south below ridge top and from the southwest above ridge top.

The second stage of convection was characterized by the apparent organization of convective elements into a coherent squall line and its movement onto the High Plains. This stage took place between 1120 and 1330 MST and appears in Fig. 18 of CGWM. During this period, increasingly intense mountain thunderstorms formed over especially favorable regions or "hot spots." Gradually, a north–south line of moderately strong radar echoes (over 40 dBZ) assembled over the foothills and moved onto the western edge of the High Plains. As the line formed it moved eastward at 10–12 m s^{-1} and began Stage 3, characterized by the eastward propagation of the convective line.

The combined surface and radar weather depiction for 1400 MST (1500 MDT) is shown in Fig. 26 of CGWM. Note the generally northwesterly flow and low relative humidities across the plains north of the Palmer Lake Divide resulting from the influence of the cold front, now stalled on the Palmer Lake Divide. To the south, the much higher surface relative humidities are evidently under the influence of generally southeasterly slope flow. At this time, the line is comprised of several very intense cells reaching TRW++, feeding primarily on moisture from the south.

As the convective line advanced totally onto the High Plains, it began to dramatically weaken and evolve from a series of intense echoes to an amorphous region of light rain and virga with only a single very small intense cell by 1600 MST (Fig. 27 of CGWM).

As the line progressed farther to the east, it again explosively developed as it passed Limon, Colorado. At this time, several regions of extreme echo intensity appeared. Behind the advancing line, surface high pressure formed, rising by as much as 0.5 kPa at 1700 MST (Fig. 29 of CGWM). Potential temperature fell by 4°–5°C behind the line, forming a distinct mesoscale front. It should be noted that surface winds immediately behind the advancing mesoscale cold front did back to a slightly stronger westerly flow but in no way reflected the 10–12 m s^{-1} movement of the convective system. The surface windflow was obviously unbalanced geostrophically with direct outflow across the isobars. In fact, the mesohigh, coincident with regions of ongoing precipitation, demonstrated no persistence as the intensity of convection fluctuated. The 20 dBZ radar echo itself moved ahead of the surface mesoscale front, and in some cases so did indicated cell centers. This is evidence that perhaps some virga was falling in advance of the primary convective line.

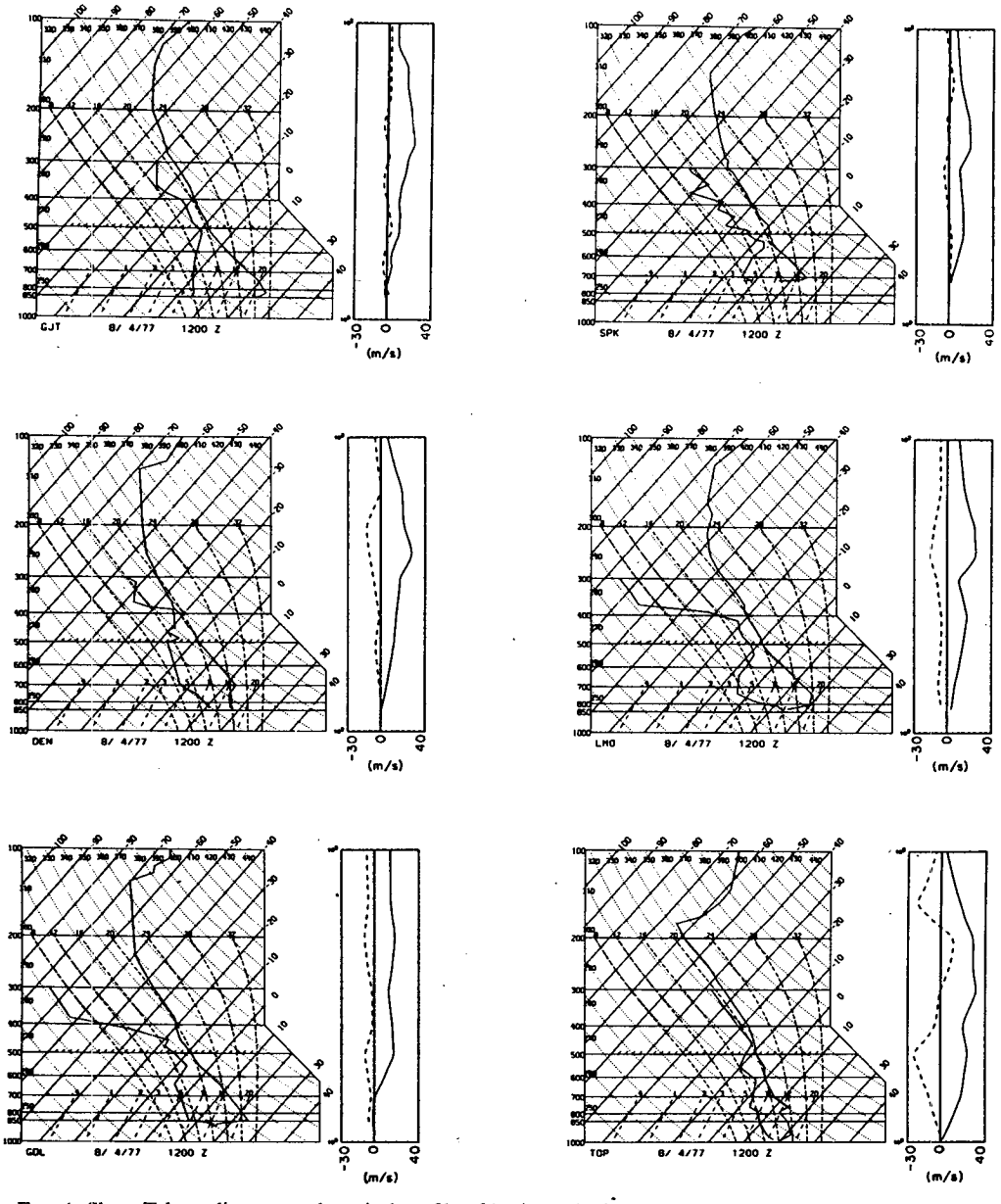

FIG. 1. Skew T–log$p$ diagram and vertical profile of horizontal wind components (u and v) from 1200 UTC sounding observations taken at six stations across the region of interest near 39°N. Temperature and dewpoint profiles are displayed. Wind vectors are displayed to the right of each diagram.

Figure 2 depicts the satellite-observed development of the line throughout the afternoon and early evening. Note the tendency for the line to favor the Palmer Lake Divide and Raton Mesa (east–west oriented ridges on the High Plains passing along the Colorado–New Mexico border) during the midafternoon. At the same time, no convection was visible along the drier Cheyenne ridge, north of the synoptic-scale cool front. However, as the system moved close to the Colorado–Kansas border by 1900 MST (2000 MDT) the line became nearly continuous in the north–south direction, even into northeastern Colorado.

Subsequently, as the system passed into Kansas and encountered greater moisture, it expanded zonally (see Wetzel et al. 1983). Figure 3 (from McAnelly and Cotton 1986) depicts the evolution of combined satellite and radar analysis after sunset. Note that as the system approached Kansas, several mesoβ-scale (20–200 km) radar echos broke out ahead of the advancing line in central Kansas. In this region, dominated at low levels by synoptic-scale southerly flow around the western extremity of the subtropical high, the low-level southerly jet intensified as nighttime ensued. With the appearance of the new mesoβ-scale convective centers

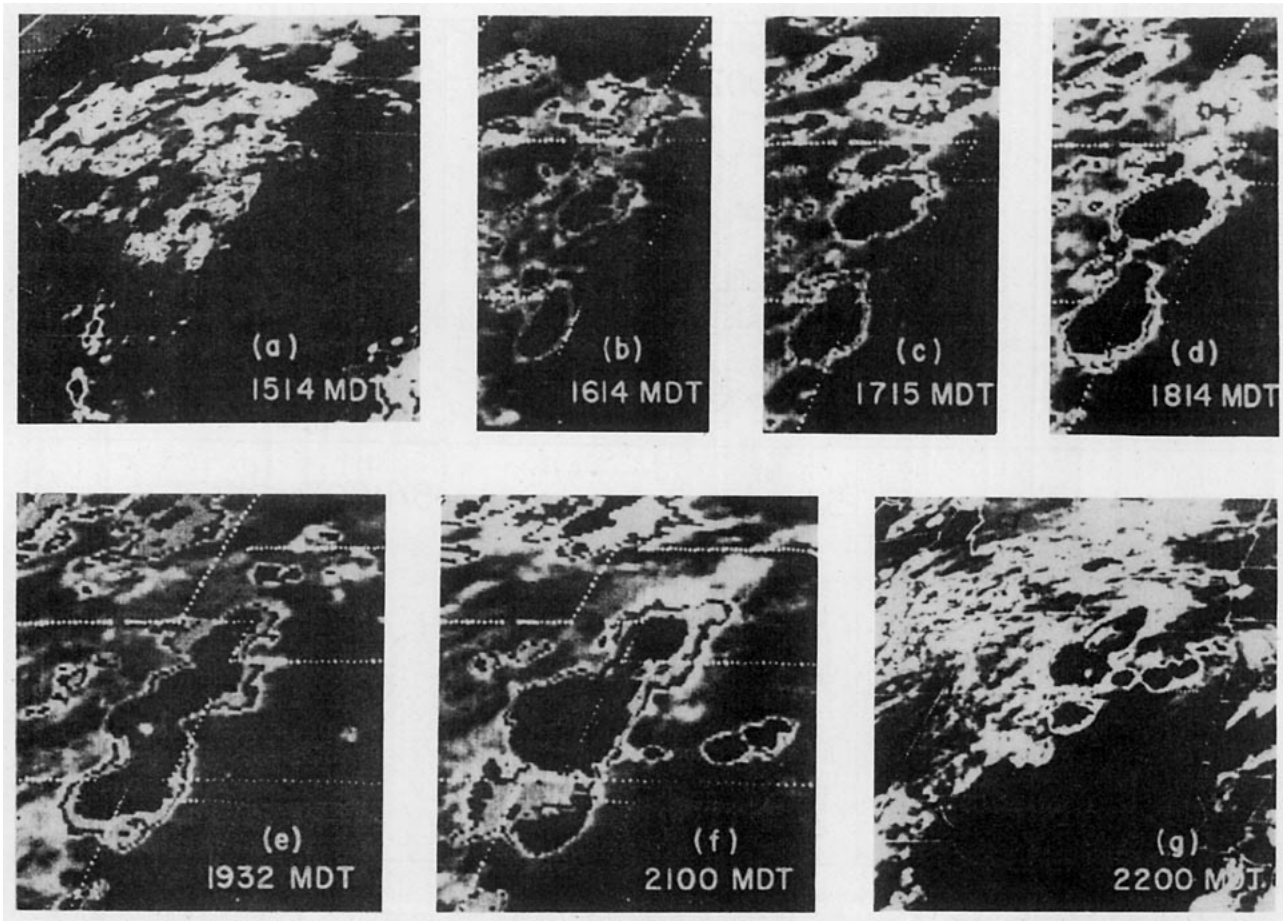

FIG. 2. Infrared satellite images, centered near eastern Colorado on 4 August 1977 for MDT times (a) 1514, (b) 1614, (c) 1715, (d) 1814, (e) 1932, (f) 2100 and (g) 2200. The first and last images, at half the scale of the others, provide more extensive views of the storm system's environment. Gray shades are as in Fig. 4 of Wetzel et al. (1983). Temperatures colder than −63°C (lighter shades within interior black contours) indicate convection reaching or penetrating the tropopause, which, based on the 1700 MDT Limon sounding was at 13.2 kPa (15.0 km). (From Cotton et al. 1983.)

just after sunset, the system rapidly evolved from the line structure to a more classical MCC shape. The new structure was ultimately characterized by several transient regions of mesoβ-scale convection beneath an encompassing anvil of low eccentricity (when viewed by satellite). This mesoβ-scale transient convection, which appears randomly organized in the horizontal plane, has been observed by the second author (Cotton) to form just after sunset.

Several important questions arise from this analysis. First, could local flow systems act to organize convection in a manner consistent with the observations and, if so, are dynamic mechanisms responsible? Second, why did it weaken as it moved onto the plains and then suddenly grow explosively? Was this an effect of the synoptic situation? Third, it can be asked: Of what relative importance were the west slope and east slope moisture sources? Fourth: How important are local slope winds to development? Was the enhanced convergence caused by the synoptic-scale cold front instrumental to development? Was the system continuously forced by mesoscale convergence associated with slope flows or did it force its own boundary-layer convergence? Fifth: Under what dynamic mechanism was the system principally organized? Was it a wave-CISK disturbance as Wetzel et al. (1983) hypothesized? Sixth: How did the organization change after sunset? Why did the system rapidly evolve into a circular anvil system with several regions of mesoβ-scale convection?

In the next section, an experimental design to answer these questions will be described.

3. Experimental design

The approach taken in this study will be to form a model of MCS orogenesis that is consistent with known theory and adequately simulates the development scenario. Of course, the definition of adequate depends on the goals of the investigation. Certainly, one cannot expect to prove our hypothesis conclusively or prove that the dynamics as proposed here are what actually took place. But using a credible numerical model, we

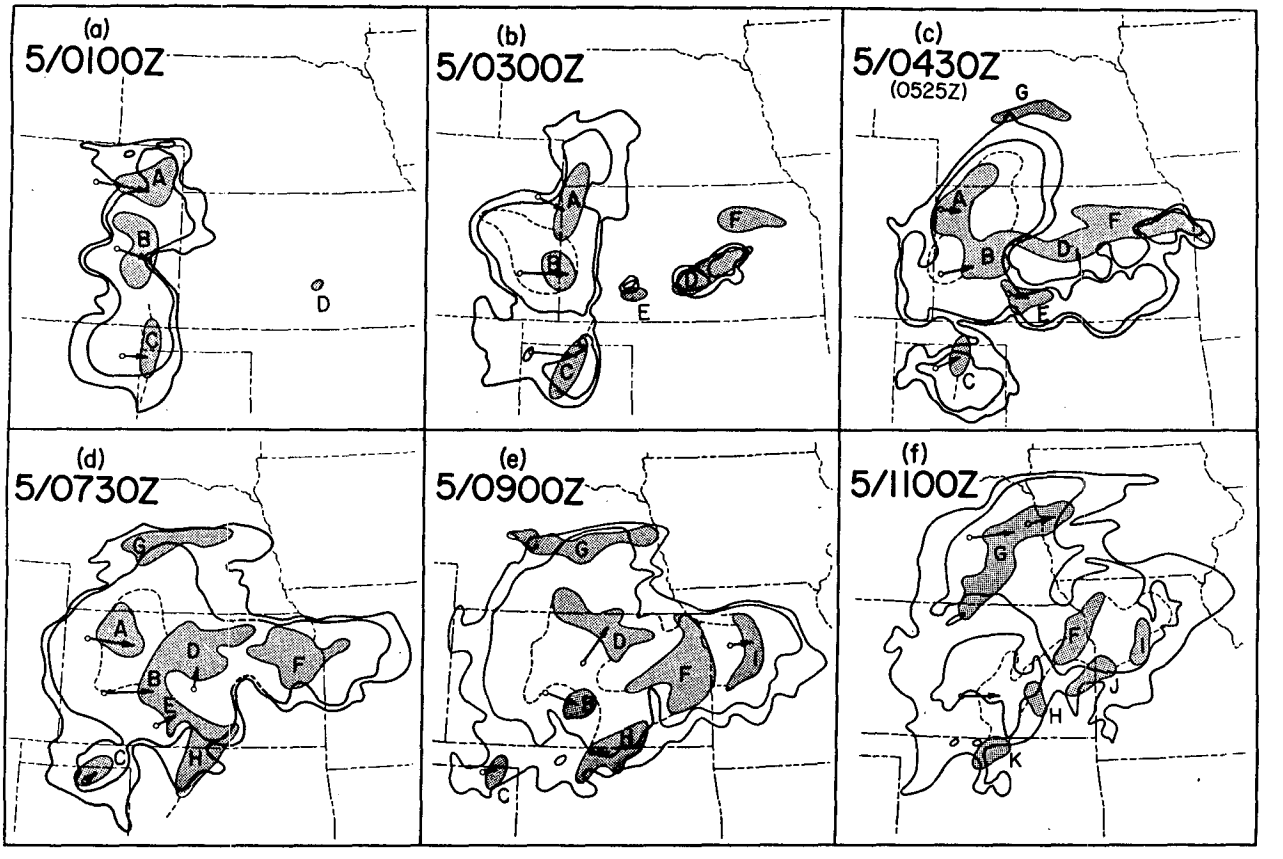

FIG. 3. Schematic IR satellite and radar analysis at 2-h intervals, from 0100 to 1100 UTC 4 August 1977, for a western MCC. The anvil cloud shields are indicated by the −32°C and −53°C IR contours (outer and inner solid lines, respectively), re-mapped from satellite images at the labeled times. Darkly shaded regions (identified by letters) denote significant radar-observed, mesoβ-scale convective features at about 25 min after the indicated whole hour, with the vectors showing their previous 2 h movements. The dashed line segments extending from the mesoβ convective features indicate flanking axes of weaker convection. In the more developed MCC stages, in (e) and (f), the light-shaded area within the dashed envelope indicates weaker, more uniform and widespread echo. (From McAnelly and Cotton 1986.)

can expect to at least support the hypothesis with consistent dynamical and thermodynamical arguments, and to the extent that one explains all the details of the observations, one can gain confidence that the dynamics were what really took place.

In numerical studies of tropical and midlatitude MCSs, it is customary to represent convection with a convective parameterization. Recently, several authors (Rosenthal 1979; Ross and Orlanski 1982) proposed that latent heating is better represented with explicit latent heating from resolvable scale flows and with simple parameterized microphysics. Others, however, argue that explicit heating presents problems in timing of onset and intensity of heating when not adequately resolved (Molinari and Dudek 1985; Redelsperger and Sommeria 1986).

In either case, there are significant dynamical inconsistencies in selecting a grid capable of resolving mesoβ-scale but not mesoγ-scale features of a convective system. Because significant transient (gravity-wave) energy is resolved, the actual cloud circulation may be partially resolved. But it is resolved too poorly to produce a realistic representation of the heating. On the other hand, there is no important scale separation between the resolved transients and the unresolved convection that would suggest a parameterization hypothesis is valid. In fact, it is not likely that compensating subsidence would even be within the same grid box as the supporting vertical motion.

Besides these inconsistencies, one should examine some known facts concerning the atmosphere's response to heating, i.e., geostrophic adjustment. Linear dynamical analysis of the governing equations reveals the important scale length called the Rossby radius given most simply by

$$L_R = \frac{C_g}{f} \tag{1}$$

where C_g is the gravity-wave phase speed and f is the Coriolis parameter. When the atmosphere is perturbed with a heat source, the atmosphere responds dramat-

ically different for scales smaller than the Rossby radius compar ed to larger scales. For scales larger than L_R, the inertial restoring forces dominate the wave dynamics and this causes the wind to come into adjustment with the mass (or temperature) field. For scales smaller than L_R, the vertical stability of the atmosphere dominates the wave dynamics and so the mass field adjusts to the wind, or transient gravity oscillations are produced. This, then, has a significant impact on the construction of a model to represent MCS genesis. If the MCS is defined as the semigeostrophic circulation, then its growth is critically dependent on the amount of heating projected on scales larger than the Rossby radius. The Rossby radius happens to be around 300–600 km for summertime midlatitude disturbances, suggesting a significant contribution to the dynamics from motion scales both greater than and less than the Rossby radius.

The selection of a mesoβ-grid scale implicitly imposes an arbitrary assumption of heating scales whether a parameterization is employed or not. Therefore, it should not be surprising for a simulation with a grid scale of 60 km to produce a semigeostrophic solution from a convective heat source simply because the heating is numerically forced to scales larger than the Rossby radius. As a result, the approach that is taken involves the development of a model that is able to simulate a large range of atmospheric scale responses to heating both larger and smaller than the Rossby radius. It is hypothesized that scale selection by the model will then be more physical and result in new insights to the scale interaction problem. Ultimately, we expect that new understandings could be used to improve parameterization techniques which we envision will be necessary for the forseeable future.

Because of finite computer resources, this choice, too, involves major compromises. In order to model the cloud scale (mesoγ-), mesoβ-scale and mesoα-scale[1] simultaneously, only a two-dimensional simulation is possible. The compromise of two-dimensionality is indeed serious and neglects some important dynamical mechanisms. In fact, it is well known that two dimensionality will cause energy to cascade in reverse to larger scales. Some impact can then be expected on the genesis process, especially on eddies within the modeled two-dimensional plane. However, because the observed developing MCS was nearly linear in the north–south direction, and because the Rockies are conveniently linear in the north–south direction, a major portion of that compromise is minimized. Another feature that cannot be represented is the ultimate development of a "circular" structure that evolved after dark. This aspect of the storm's evolution will be left for future studies. Instead, we will concentrate on the development of the linear structure displayed in the early phases of the MCC.

The model used is an extension of the nonhydrostatic primitive equation cloud model with explicit microphysics described by Tripoli and Cotton (1982) and modified by Tripoli (1986). Predicted variables include the three Cartesian velocity components (u, v, w), perturbation exner function (π'), ice–liquid water potential temperature (θ_{il}, see Tripoli and Cotton 1981) total water mixing ratio (r_r), ice crystal mixing ratio (r_i) and graupel mixing ratio (r_g). Vapor mixing ratio (r_v), cloud water mixing ratio (r_c) and potential temperature (θ) are diagnostic (see Tripoli and Cotton 1982).

A dry reference state is assumed that is hydrostatic and geostrophic. It should be noted that an inconsistency exists in the model formulation because, although a reference state exner function is assumed to be in geostrophic balance, the shear in the zonal wind implies that a meridional temperature gradient should be present, but it was not included in the model formulation. If retained, we would have included a meridional advection of base state θ_{il} into the equations. Also, since we assume an initial "v"-component close to zero, the neglected zonal temperature gradient is small. In our initial testing of the model, we did include a meridional temperature gradient, but, we found that over the long time period of integration the unbounded nature of this term led to instability and so we abandoned its use. To include this effect correctly would require representing the larger mesoα-scale meridional fields, which is beyond the scope of this paper. The reader should therefore be aware of this limitation when interpreting the results. The model includes physical parameterizations for microphysics (Cotton et al. 1982), long-wave and shortwave radiative tendencies on θ_{il} (Chen and Cotton 1983), and the surface-layer fluxes of heat, vapor and momentum (Louis 1979). Longwave and shortwave radiative fluxes are computed in cloudy regions by assuming all condensed water is in the liquid phase. The radiative effects of the ice phase are ignored. Soil temperature and soil moisture are predicted with an underlying soil model described by McCumber and Pielke (1981) and a surface energy balance model described by Tremback and Kessler (1985). Vertical and horizontal turbulent eddy mixing is modeled using an eddy viscosity approach similar to that described by Tripoli and Cotton (1982) but modified by the addition of an additional buoyancy enhancement term proposed by Hill (1974) and an improved vertical scale-length diagnostic scheme de-

[1] Orlanski (1975) proposed that the mesoscale be divided into the three scales of mesoα, mesoβ and mesoγ. The mesoα-scale represents scales from 200–2000 km and for midlatitudes would generally be scales near but larger than the Rossby radius. The mesoβ-scales are from 20–200 km, which in midlatitudes would be the transients (gravity wave motion) at scales larger than individual cumulus but smaller than the Rossby radius scales. The mesoγ-scales, on the other hand, range from 2–20 km, which could represent the motion scales of individuals cumulus towers but more generally represent transient scales where inertial effects (due to Coriolis) become secondary.

scribed by Tripoli (1986). As with any truncated numerical model, the use of a turbulence parameterization to close the model is a severe limitation. However, we and others have demonstrated that a reasonable depiction of cloud dynamics is possible with these closures. Perhaps a greater limitation is the two-dimensional structure of simulated clouds shown by Cotton and Tripoli (1978), Schlesinger (1984) and others to poorly represent some aspects of deep convection. These equations are solved on a standard velocity, staggered grid described by Tripoli and Cotton (1982). A terrain-following sigma-z vertical coordinate system is applied using the system developed by Gal-Chen and Sommerville (1975a,b).

The vertical boundary conditions are for vanishing grid-scale vertical fluxes and parameterized (Louis 1979) turbulent vertical fluxes at the surface. The top boundary condition is the normal mode gravity-wave radiative technique described by Klemp and Durran (1983). For lateral boundary conditions, gravity-wave radiative conditions described by Klemp and Lilly (1980) and modified by Durran and Klemp (1982) are employed together with a mesoscale compensation region outside the simulation domain (Tripoli and Cotton 1982). For a more detailed description of the model formulation and numerics, the reader is referred to Tripoli (1986) and the studies mentioned above. The grid has 1.08 km horizontal resolution and 250 (low-level) and 750 m (free atmosphere) vertical resolution reaching an elevation of 17.25 km AGL. Topography is a highly filtered form of the actual topography running along 39°N latitude from 50 km west of the Colorado/Utah border at 110°W to central Kansas at 98°W. This is the latitude of the Palmer Lake Divide, where the convective system was observed. Figure 4 compares the smoothed topography that was used to the actual topography sampled at 30″ longitude intervals.

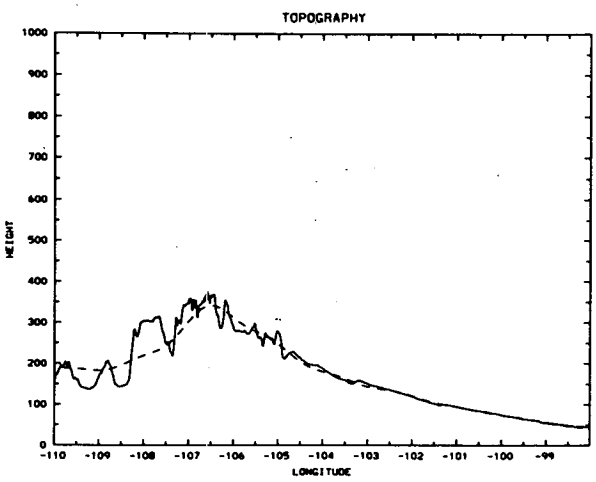

FIG. 4. Input topography sampled at 30″ longitude intervals before (solid line) and after (dashed line) filtering. Vertical axis is height meters MSL.

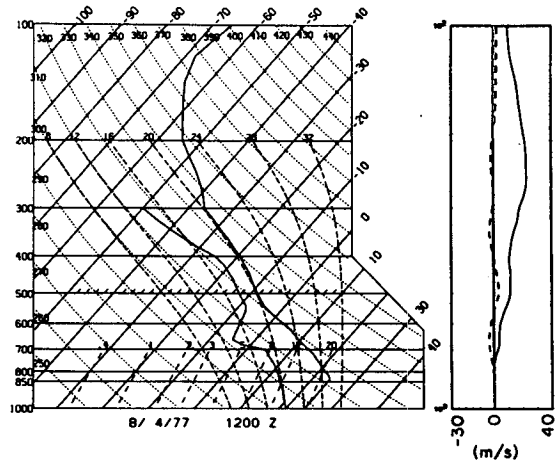

FIG. 5. Skew T-log$p$ diagram and vertical profile of horizontal winds for composite sounding for 1200 UTC 4 August 1977. Temperature and dewpoint are displayed. Wind is plotted in m s^{-1}.

The initial thermodynamic and wind conditions were specified by direct interpolation from a composite sounding representative of the gross conditions observed by the sounding network. Figure 5 depicts the composite sounding and wind profile. The composite sounding was based on the upstream Grand Junction 0500 MST observation above 70 kPa. Below 70 kPa, moisture and temperature were derived from surface observations along the east beginning with South Park at 72 kPa and ending with Topeka at 96 kPa. The composite sounding was then hand smoothed so that small features were removed.

The initial model variables were determined by first interpolating with respect to pressure from the composite sounding. In order to crudely represent the effects of a boundary layer, the surface moisture of the lowest 1 km was then set to the surface value. The justification for this was that each observed sounding had a boundary-layer where the moisture content was substantially higher than at the same elevation within the free atmosphere above a station with lower surface elevation. This represented that effect.

Temperature, however, was not changed from the composited value because the compositing technique already produced a stable lower atmosphere and we expected the nocturnal flow regime to adjust the thermal fields properly.

The observed zonal and meridional wind below 70 kPa showed no consistent features from one station to the next among the morning soundings. Therefore, we elected to force the composited sounding wind to vanish below 70 kPa with the expectation that drainage flows would develop on their own. The winds were added into the model integration using a "dynamic initialization" technique described by Cotton et al.

(1986). In short, the wind is added gradually over the first 30 minutes of integration in order to inhibit shocking the model.

The simulation began at 2000 MST (2100 MDT) on the day before expected development and then integrated for 30 hours to 0200 MST on the night of the disturbance. This allowed the development of a nocturnal inversion before the thermal upslope, which Hughes (1978) suggested is important to properly simulate the slope flow evolution.

4. Results and comparison with observations

a. Development of initial hot spot convection

As expected, without the development of a daytime planetary boundary-layer and slope flow regimes, no condensate formed during the first night. Instead, local surface flows evolved as the ridge cooled. A relatively strong leeside downslope occurred, supported by downward momentum transport from aloft. The downward motion associated with the transport was part of a deep mountain-wave system with a vertical wavelength of about 8 km. The vertical motion within the lee wave pattern had an amplitude of 1 cm s^{-1}, with the axis of peak upward motion intercepting the ridge top level at about 105.7°W and those of peak downward motion intercepting the surface at 106.5°W (ridge top) and 105°W. The vertical motion below 3.5 km MSL was dominated by drainage flow on the east slopes. The vertically propagating wave structure is strongly apparent throughout the night and the morning until deep convection begins. During this period, the surface downslope flow in the immediate 50 km lee of the Continental Divide remained nearly constant at 5 m s^{-1} despite the changing diurnal flow system. This is interpreted as evidence that the flow dynamics in this region were dominated by downward momentum transport of the mountain wave.

Associated with the drainage flows was the appearance of low-level meridional flow directed to the right of the downslope flow. Meridional flows were on the same order or exceeded the drainage winds at 0400 MST. They opposed further acceleration of the drainage winds by tending toward a geostrophic balance with the zonal pressure gradient. Later, as the baroclinically induced pressure gradient weakened as surface heating began, the meridional wind played a role in accelerating the developing upslope flow. The meridional flow seemed to have become relatively steady by this time (0400 MST) and so its effect upon the onset of upslope flow should be realistic. This would not have been simulated well had the simulation begun in the morning.

The sun rose about 0500 MST. By 0800 MST, soil temperatures increased to near their initial levels. The ridge-top surface air temperatures warmed only to their 0400 MST levels, while valley and High Plains temperatures were still 1–2°K cooler than the 0400 MST values. Nevertheless, approximate geostrophic balance between the simulated meridional wind and the horizontal pressure gradient was upset, resulting in weakening of the drainage flows on both the lee and windward side of the ridge. In fact, upslope flow was already occurring on the windward slopes where the downslope flow was opposed by the ambient wind. Because of the relatively coarse vertical grid resolution, the weakened downslope flow on the lee side can be interpreted as the development of very shallow upslope flow beneath a deeper, persisting combined drainage and ambient flow as observed by CGWM. The consequence of coarse vertical resolution was that any upslope transport within the strong gradients of the surface layer could not be resolved explicitly. Nevertheless, the slowing of the mean westerly flow reduced the larger mean transport, partially reproducing the observed effect. To the extent that the return branch of the shallow circulation was contained within the lowest grid layer, however, the simulation would be in error. This, likely, had a minimal effect on the large-scale transports because this flow regime was very shallow and short-lived, so transport over large horizontal scales was not likely.

The thermally driven upslope flows continued development in conjunction with increasing soil temperature throughout the morning. It was not until 1130 MST that the first shallow convection formed. The observations of CGWM demonstrated that the first convective elements occurred as much as 1 hour earlier. The reason that convection occurred late in this simulation can be explained as follows.

The initial convection in this simulation, displayed in Fig. 6, was forced by the interaction of the large-scale flow with the shallow valley breeze on the scale of the entire ridge. This was because all small-scale peaks were removed in this idealized topography, which eliminated hot spots (Henz 1974). Cotton et al. (1983) attributed early convective elements to such small-scale topographically forced circulations. During initial testing for this numerical experiment, a simulation was run where short wavelength topography was included. In that case convective elements did form by 1030 MST over isolated peaks. This suggests that hot spots significantly augment the evolution of early convection and hasten the development of the entire first stage of the mesoscale system.

From Fig. 6, it can be inferred that the formation of a cloud over the ridge-top was associated with the upslope advection of moisture from the west to cloud base. Comparison of this with the moisture pattern of dawn suggests that the increased windward upslope advection at noon was forced by the combined effects of thermally driven upslope and ambient westerly flow over the ridge. A comparison of west slope moisture to east slope moisture at 3 km MSL shows that considerably higher moisture existed on the west slope.

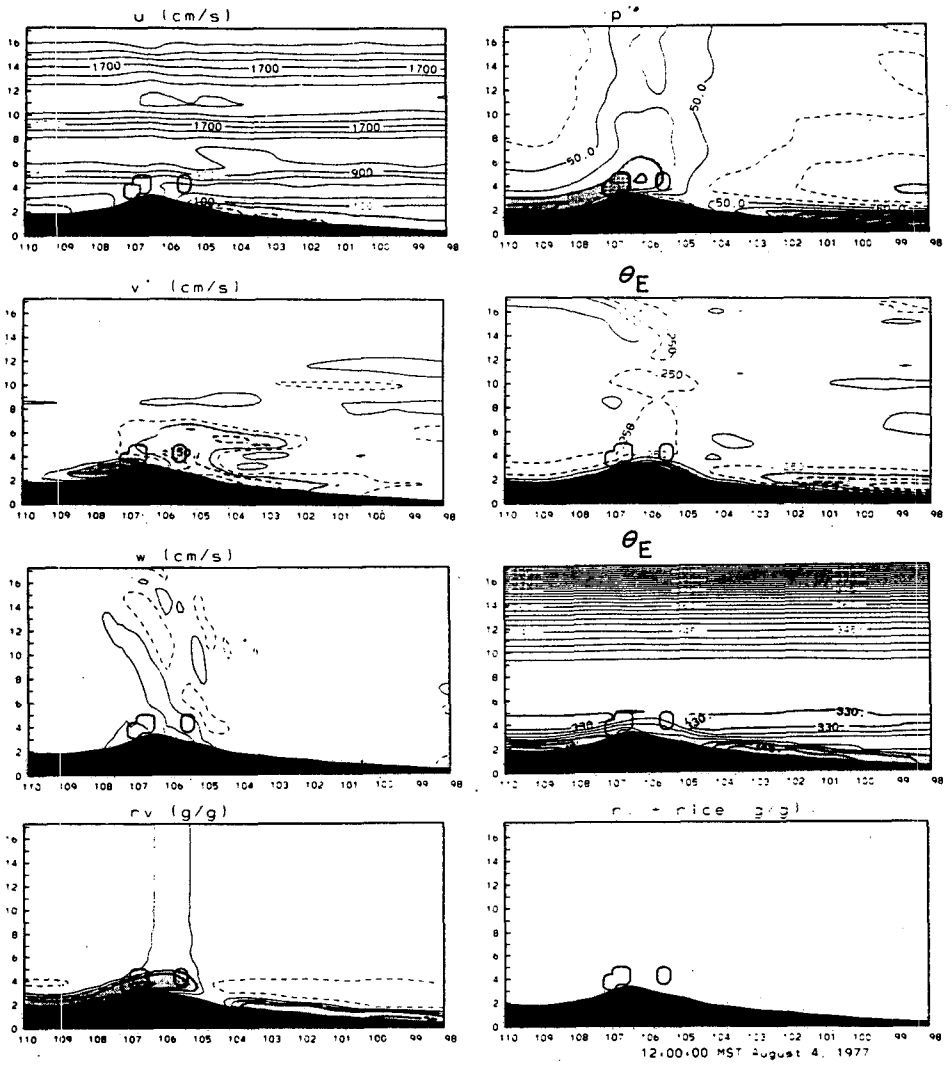

FIG. 6. Predicted mesoβ-scale fields at 1200 MST for control case. Variables are as labeled. Heavy (medium) shading is used to emphasize large (small) values at a given threshold. The fields represent 80 grid point (86 km) running averages of actual predicted variables. The variables, r_v, p' and θ' have their horizontal average removed. The variable v' represents the change from the reference state (initial) meridional wind. Contour intervals are 2 m s^{-1} (labeled as 200 m s^{-1}) for u and 1 m s^{-1} for v', 1 g kg^{-1} for r_v, 1 mb (100 dyn cm^{-2}) for p', 0.5 K for θ', 3 K for θ_e and 0.5 g kg^{-1} for condensate. Only the ± 1 and ± 5 cm s^{-1} contours are drawn for w. Negative contours are dashed and the zero line is placed between intervals for those not positive definite. Upper and lower emphasis thresholds are none and 0.0 m s^{-1} for u', ± 3 m s^{-1} for v', ± 5 cm s^{-1} for w', none and 1.5 g kg^{-1} for r_v, ± 3 mb for p', ± 0.75 K for θ', 339 K for θ_e and 1 g kg^{-1} and none for condensate. The boundary for condensate in excess of 0.01 g kg^{-1} (cloud boundary) is drawn by a heavy, dark line, and the region within is lightly shaded. The surface topography is depicted by the black shading. The vertical axis is height in km above MSL and the horizontal axis is west longitude. The vertical distance is exaggerated by a factor of 30.

Observationally, such moistening has been linked to the Southwest Monsoon (Hales 1972; Culverwell 1982), which was operating on this case study day.

The second region of cloud formation (see Fig. 6) was associated with a reversal of the surface horizontal flow 60 km to the east of the ridge-top (105.7°W longitude). Note the continuity of westerly flow from aloft down to low levels just to the lee of the ridge. It is significant that this westerly flow persisted at 5–6 m s^{-1} (which is 3–5 m s^{-1} stronger than the ambient flow) from the nighttime hours in this region. Recall that this region of westerly flow was attributed to the mountain-wave-induced momentum transport, which was evident well before sunrise. Moreover, the region

of mesoβ-scale upward motion is coincident with the point where the axis of rising motion associated with the mountain wave intersects the surface. This suggests that the mountain-wave plays a role in organizing this region of cloud formation. Note that the high water-vapor mixing ratios of the plains were not yet transported westward to the elevation of the convergence zone (almost 3 km MSL) and that the primary source of moisture supplying the early convection is from the west.

Although the mountain wave and thermally driven slope flow interaction produced a region of shallow convergence and resulting mesoβ-scale vertical motion pattern near the eastern convection regime stronger than that at ridge top, the ridge-top convection dominated at first because of greater moisture advection from the west. The region of leeside convergence represents the up-branch of a shallow (5 km) mountain–plains solenoid circulation that was developing. The θ' pattern, displayed also in Fig. 6, shows that the air was relatively warm near the surface and was cooler just below the inversion. This occurred largely due to adiabatic cooling of the upslope flow. Near the surface, the cooling effect was overwhelmed by solar heating. Note that the easterly flow regime was confined to beneath the plains inversion, which can be located by the packing of r_v *and* θ_e contours above the mixed layer. Above the inversion, subsiding westerly return flow acts to warm ambient conditions. Together, the eastward and westward branches of the solenoid act to strengthen the plains inversion.

b. Initial mesoscale organization of convection

By 1245 MST, the ridge top convection was the first to deepen to the tropopause. The eastern zones of initial shallow convection eventually deepened to the tropopause by 1300 MST but with less vigor. The mesoβ-scale vertical motion and perturbation potential temperature fields for 1300 MST are displayed in Fig. 7. Note that the deep convection developing near the ridge top was considerably stronger, both in vertical motion and warming.

From Fig. 7, an important result of competition between the two regions of convection can be clearly seen through the mesoβ-scale vertical motion field associated with the convective tower. It is significant that the region of weak upward vertical motion runs just in advance (east) of the cloud boundary, with a region of relatively stronger subsidence laterally to the west and another region of weaker subsidence ahead of the upward vertical motion. Moreover, the low-level surface convergence has remained at the original location 60 km east of the ridge top and continues to force strong, low-level upward vertical motion.

We suggest that the following scenario led to this behavior: The greater moisture associated with the ridge top convection allowed stronger and more rapid development, causing the lee side regime to grow within a zone of upper-level forced subsidence. The subsidence was forced by a vertical pressure gradient transmitted from the western dominant convection. This weakened the ability of the eastern convection to develop. As a result, the mesoβ-scale impact of the eastern convection was overwhelmed by that of the western convection, causing it to further stagnate. The eastern displacement of the vertical motion field from the cloudiness reflects the suppression from the west.

As convection penetrated the stronger upper-level flow, the deep mesoβ-scale response began to drift eastward. Because its upper-level heating was relatively weak, the low-level solenoidal circulation continued to be dominated by the low-level baroclinicity and mountain-wave effects induced by the sloped terrain. This was evidenced in the pressure field where lowest surface pressure was still found east of the most active convection in the region of the up-branch of the slope circulation. The effects of upper-level convective heating were beginning to be felt, however, as evidenced by the deep mesoβ-scale solenoidal cell developing near ridge top.

As the eastern convection drifted eastward sufficiently far from the forced subsidence of the ridge top convection, the suppression was reduced and the convection experienced renewed growth. By 1500 MST (see Fig. 8), a rather dramatic transformation took place. As the region of eastern convection moved east of the mountain-wave convergence zone and over the plains inversion, it rapidly weakened as it decoupled from the surface moisture supply. As the core up-branch cooled, the mesoβ-scale circulation broke into oppositely propagating gravity-wave pulses. The amplitude of these waves dissipated by more than 80% after traveling just one horizontal wavelength in the lower troposphere. The wave phase lines suggest wave energy was propagated upward into the stratosphere. Remnants of the eastward-propagating gravity wave were visible for several hours following breakup, as it moved over the plains inversion.

As the original ridge top convection moved over the mountain-wave convergence zone from the west, explosive growth took place. Strong upper-level (35 kPa or 8 km) mesoβ-scale heating of nearly 3°C developed, inducing low pressure between the 50 and 80 kPa pressure levels, while evaporating precipitation-induced cooling increased surface pressure. At the same time, upper-level high pressure strengthened, forcing increased outflow.

The high pressure near 4 km MSL associated with the mountain–plains solenoid was replaced by low pressure induced by the cumulus heating. At the same time, the pressure high reformed at near 20 kPa, apparently from the cumulus-induced upward mass transport. In effect, the mountain–plains solenoid be-

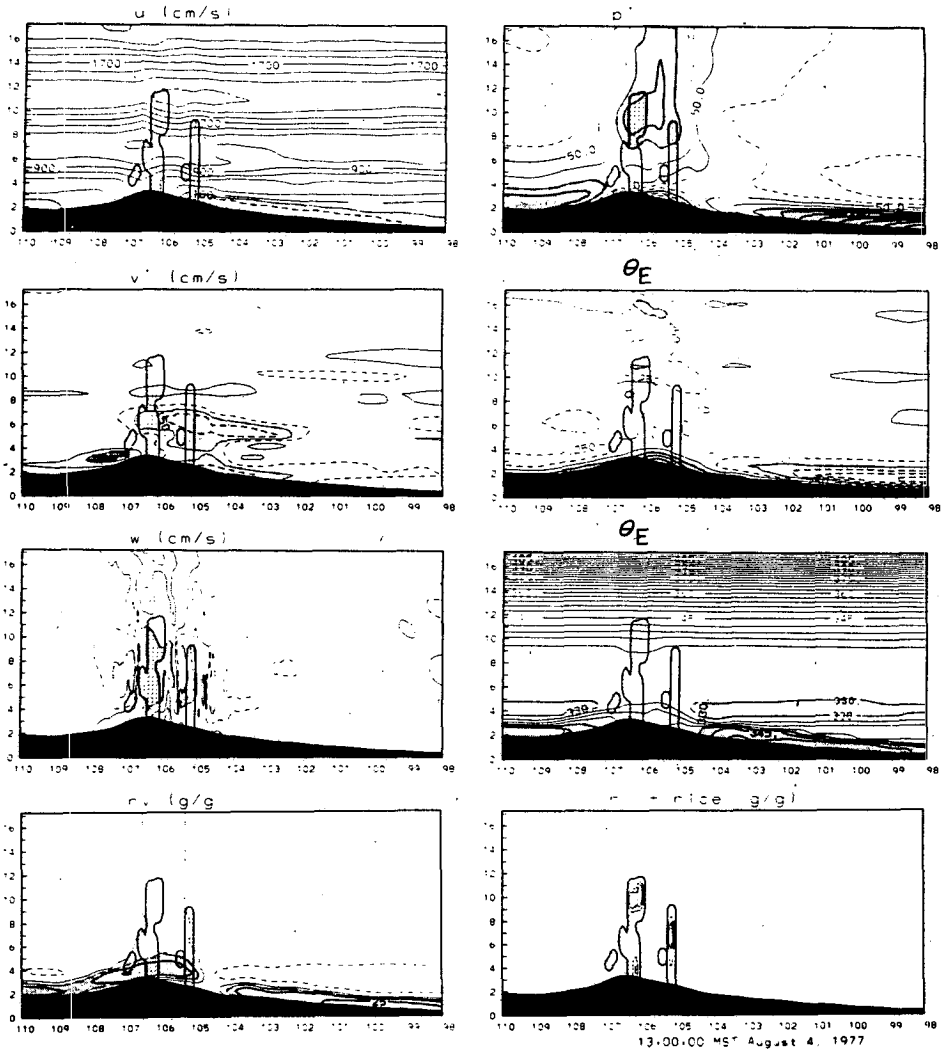

FIG. 7. As in Fig. 6, except for 1300 MST and a cloud boundary threshold of 0.01 g kg^{-1}.

came dominated locally by the convection-forced pressure gradient. At these early stages, deep compensating subsidence was confined primarily to within 150 km of the up-branch. After some time, it will be shown that some of the compensating subsidence will be found 300–400 km from the up-branch, suggesting the growth of a deep mesoα-scale solenoid.

The growth of the deep mesoα-scale solenoid can be seen in the streamline evolution. The streamfunction is defined:

$$\rho_o(u - u_r) = -\frac{\partial \psi}{\partial z} \tag{2}$$

$$\rho_o w = \frac{\partial \psi}{\partial x} \tag{3}$$

where ψ is the momentum streamfunction, u_r the storm motion, and ρ_o the reference state density. To display the streamfunction, the above equation is solved for ψ using the boundary conditions:

$$\begin{aligned} \frac{\partial \psi}{\partial x} &= 0 \quad \text{(lateral boundaries)} \\ \psi &= 0 \quad \text{(surface)} \\ \psi &= \psi_l, \quad \text{(upper boundary)} \end{aligned} \tag{4}$$

where ψ_l is integrated from the lower west corner clockwise using the relation:

$$\frac{\partial \psi}{\partial l} = v_n. \tag{5}$$

The momentum normal to the boundary is v_n and l is the path length, positive in the clockwise direction. For momentum conservation, the u-component below topography is assumed to vanish. The streamline evolution between 1300 and 1600 MST is displayed in

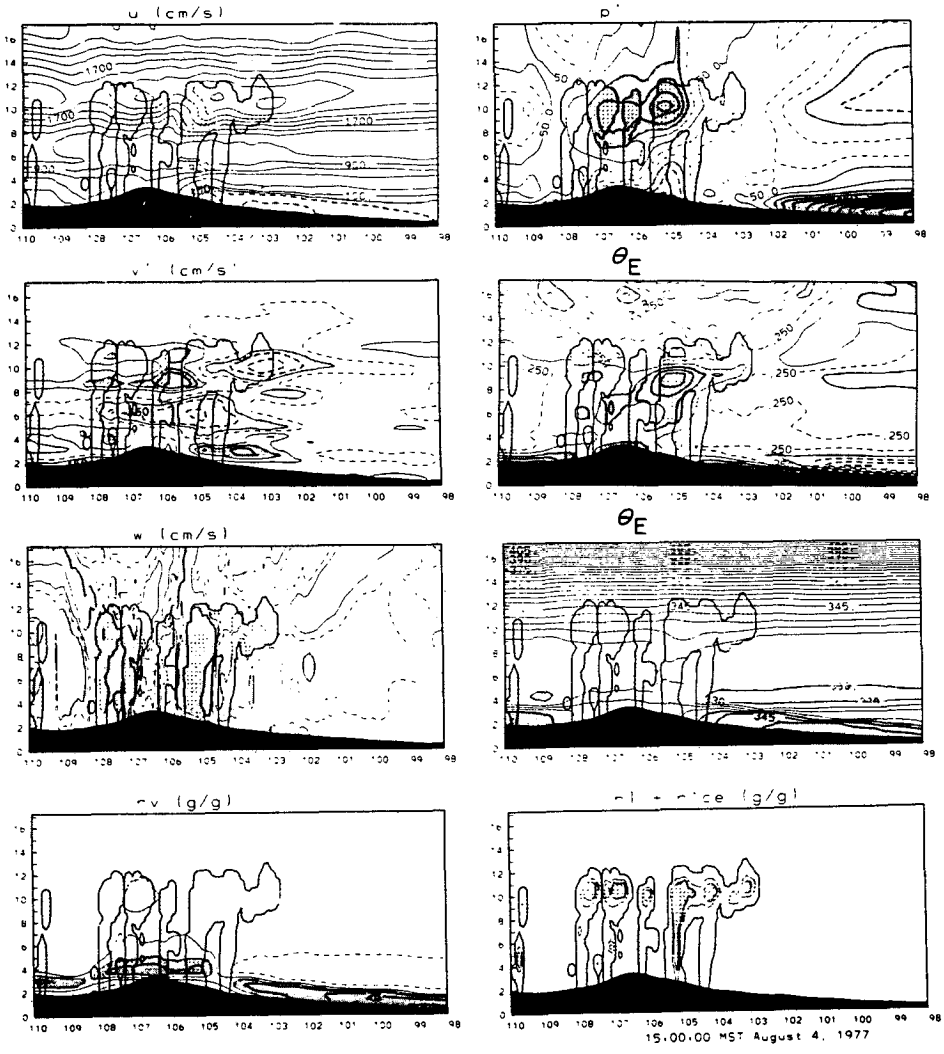

FIG. 8. As in Fig. 6, except for 1500 MST.

Fig. 9 with an assumed storm movement of $u_r = 10$ m s^{-1}, calculated by tracking the movement of the primary precipitation shaft. Note the explosive growth of the up-branch near 105°W, especially between 1500 and 1600 MST. It is evident that there is very little alteration of the mesoα-scale flow field until after 1500 MST, when a significant expansion of the mesoβ-scale subsidence seems to occur. The increase in mesoα-scale outflow and inflow, evidenced by the number of streamlines entering the circulation from distances greater than 300 km from the up-branch, can be seen to occur beginning at 1500 MST.

It is also apparent from Fig. 9 that as the primary mesoβ-scale up-branch developed, convection occurring in surrounding regions became suppressed. This is evidenced by the dramatic decrease in the frequency and intensity of convection outside of the mesoβ-scale up-branch by 1600 MST. The formation of a substantial mesoβ-scale and the beginning of a mesoα-scale circulation marks the transition to Stage 3, described observationally by CGWM.

As in the model simulation, explosive growth into a squall-line-like structure was observed to occur in the region just east of South Park. Recall that this stage appeared in the observations some 1.5 hours earlier than in the simulation, but under essentially the same scenario. It has also been shown in a climatological sense by Phillip (1979) that the suppression of surrounding convection at the time of transition is common. Although this stage was marked by CGWM as the beginning of propagation, these numerical experimental results suggest that it is perhaps the beginning of the controlling influence of a single mesoβ-scale up-branch on the distribution of individual convective elements. This would give the appearance of the beginning of propagation, but the eastward shift of con-

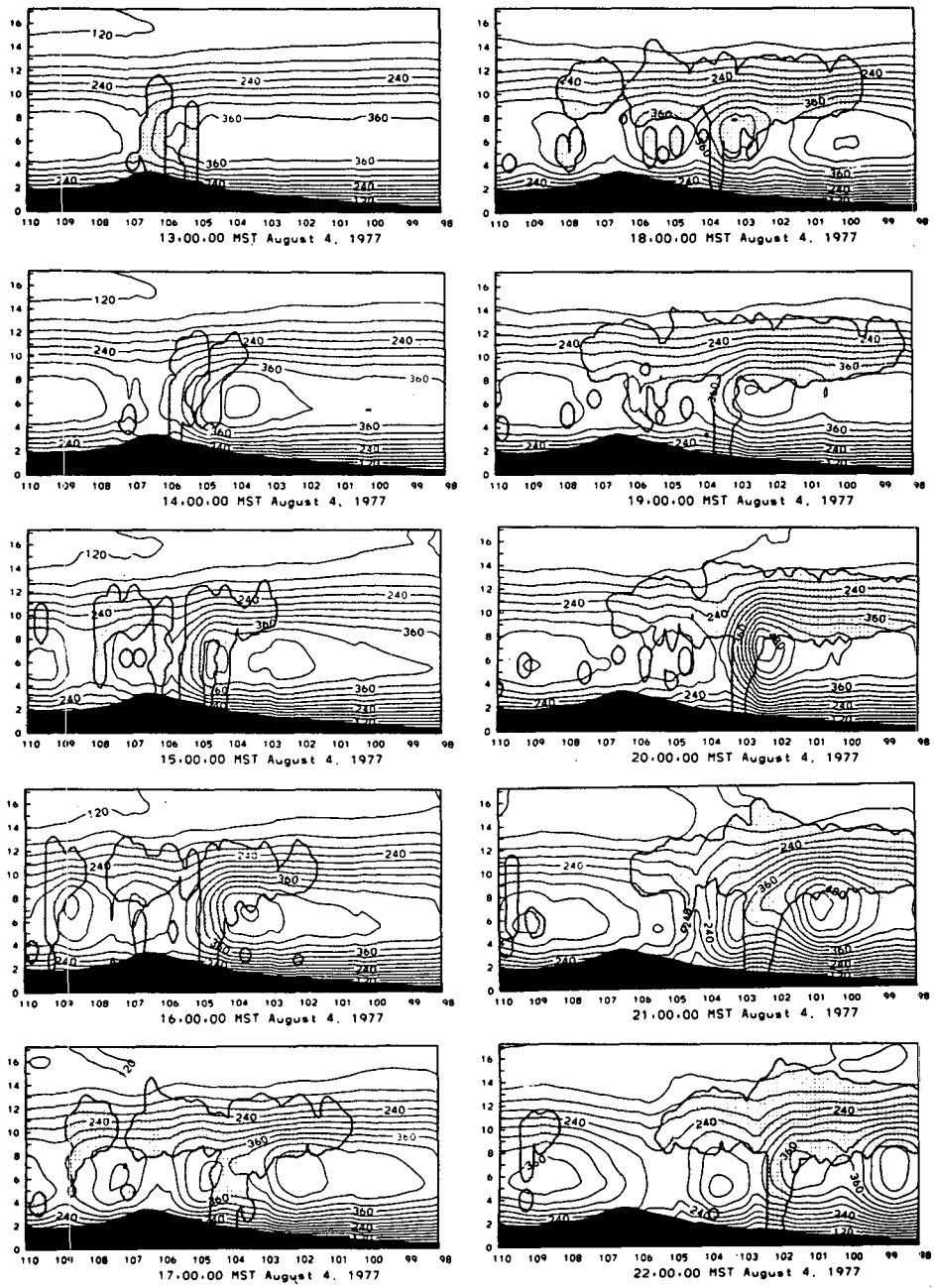

FIG. 9. Streamline fields at times displayed (MST), based on 80 grid point (86 km) running averaged storm relative wind field. For the purposes of this plot, storm movement is defined to be 10 m s^{-1}. Contour interval is 500 g cm^{-1} s^{-1}. Cloud depiction, vertical and horizontal axes, topography and exaggeration of vertical coordinate are as in Fig. 5.

vection may be a result of the dominance of the mesoβ-scale organization on the location of convective hot spots.

It is evident from Fig. 9 that the calculated storm movement of 10 m s^{-1}, which was subtracted from the flow in order to form the streamline pattern, effectively divides the flow field equally between easterly and westerly momentum. This clearly demonstrates that the calculated movement represents the mean tropospheric flow. The storm movement may have been a result of the convection itself, which in the early stage after deepening moved with a similar velocity. It should be noted that without deep convection, the deep mesoβ-scale circulation would be an indirect thermal circu-

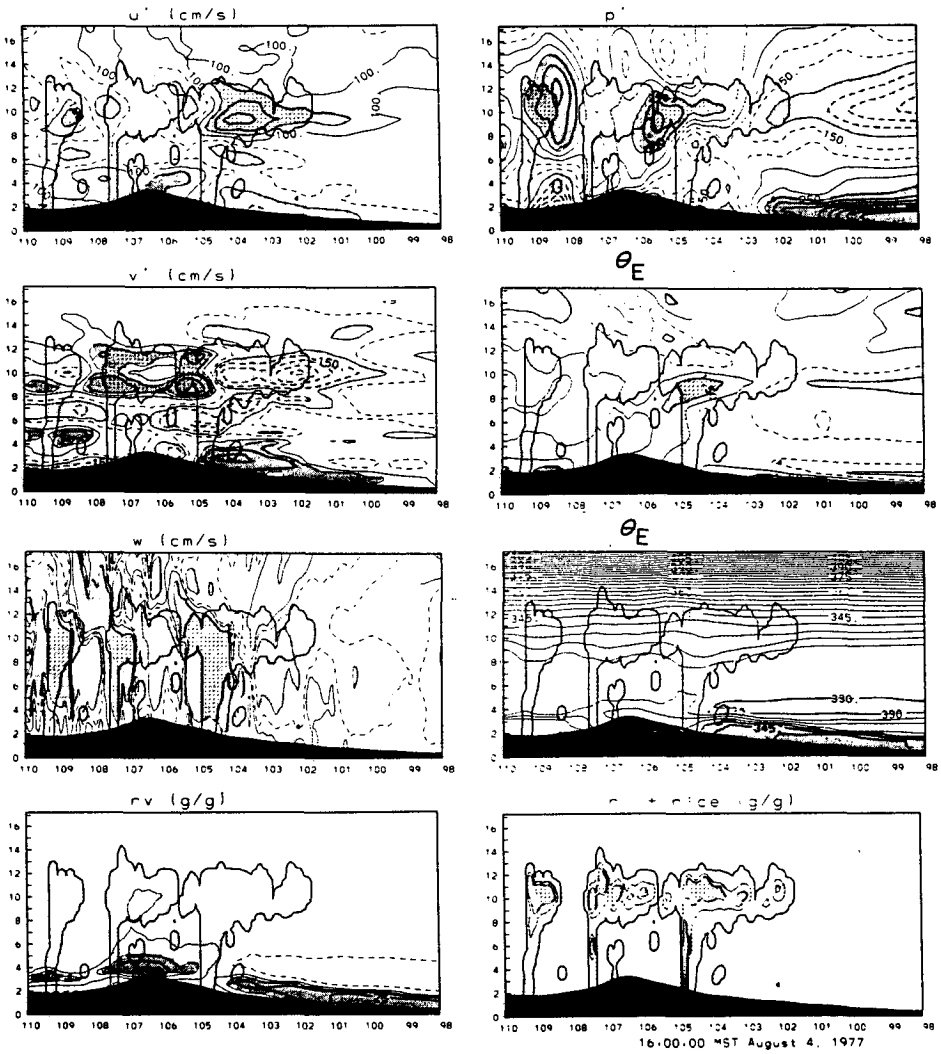

FIG. 10. As in Fig. 6, except for 1600 MST and u' is drawn instead of u. Regions of u' greater than 3 m s^{-1} are emphasized with heaving shading while those having u' less than 3 m s^{-1} have medium shading. Also θ' interval changed to 1 K and thresholds for emphasis are ±1.5 K.

lation. Unstable moist convection makes the up-branch a direct circulation and as such supplies energy to increase the circulation as a whole.

The mesoscale structure of the thermodynamic field at 1600 MST is displayed in Fig. 10. This represents the period of peak intensity during the early phase of development when plains moisture was moving into the base of the system. Strong warming at 30 kPa was apparent and strong cooling above the core was seen. In conjunction with the strong 20 kPa cooling, a vertically propagating stratospheric gravity wave above the up-branch was apparent as ambient flow moved over the convection. This effect is probably somewhat exaggerated in this two-dimensional framework. It is interesting that strongest low-level pressure deficit was induced ahead of the system and sloping upward toward the west, despite the deeper warming to the rear of the up-branch. This seems to have been caused mainly by the westward-sloping cooling aloft.

Note also the virga that was falling ahead of the system over the inversion. The formation of virga in advance is found often in these simulations, and the author's personal observations of these systems support its climatological existence. In fact, the observations of CGWM of this case document significant radar returns in advance of the surface system. Its existence in advance of the system is also reflected in the lack of deep warming ahead of the mesoβ-scale up-branch despite significant subsidence. Closer examination of more of the model output suggests that this virga may be an important contributor to the erosion of the capping inversion.

c. Evolution of the orogenic squall line

It was at 1600 MST that the simulated mesoscale system moved onto the eastern plains from the foothills of the Rocky Mountains. This marks a critical point in the system evolution because it is here that the first major breakdown of the mesoβ-scale up-branch began to occur. Note that the upbranch, located at 105°W, had access to increasingly warm θ_e as it moved eastward. Although the warmer θ_e levels supported increased growth, other evidence suggests that the peak intensity was modulated strongly by the mesoβ-scale flow dynamics. For instance, explosive growth first began about 1430 MST not with a sudden increase of θ_e, but with the mesoβ-scale mountain-wave convergence zone. Just after 1600 MST, a major collapse of the upbranch began, although Fig. 10 showed only increasing θ_e to the east.

We ask: What caused the mesoβ-scale circulation to collapse by 1630 MST? As Dirks (1969) demonstrated, the strong change in the slope of the topography around 105°W produces an acceleration of the thermally driven slope flow to the west. Moreover, as Dirks et al. (1967) predicted and as we found earlier in this simulation (see Fig. 6c for instance), this is also a region of mountain-wave-induced subsidence. These effects result in a natural tendency for surface divergence near 105°W. We find evidence that it is this tendency that led to the breakdown of the mesoβ-scale circulation.

Raymond (1983) found that breakdown of the advective wave-CISK mode occurs at the critical point where the downward cumulus mass flux becomes less than the upward cumulus mass flux in the wave. Alternatively, we may view this as the point where the heat flux demanded by the upbranch exceeds that supplied by surface convergence. If, before breakdown, the two fluxes are in approximate balance, only a small change is necessary to initiate breakdown. We believe that the surface divergence of slope flow at 105°W provides such a change.

Physically what appears to have taken place is the following: The slightly weakened surface divergence at 105°W forced increased dynamic entrainment from above the plains inversion into the mesoβ-scale updraft. The cooler updraft led to increased surface pressure, which further decreased surface convergence and so on. As Raymond (1983) predicted, the collapse produced oppositely propagating gravity-wave modes. The early stages of breakdown were already apparent at 1600 MST (Fig. 10) by the fact that the relative low found at the surface at 1500 MST had ascended to 70 km AGL.

By 1630 MST, a surface high-pressure dome developed with an excess pressure of about 0.06 kPa over surroundings. This pressure rise was less than that found in the observations, where the pressure rose by as much as 0.3 kPa behind the surface mesofront. The strong observed pressure rise was not reproduced, in part because of the two-dimensionality, which will tend to represent an average rise (the observed average rise was closer to 0.2 kPa), and because the observed postfrontal surface pressure rise is strongly exaggerated when reduced to sea level, especially when considering that the surface cool pool is rather shallow.

The resulting surface divergence led to a major weakening of the system, characterized by peak updraft speeds falling from 15 m s^{-1} at 1530 to 2 m s^{-1} at 1630. Also, the surface divergence beneath the primary MCS reestablished the easterly flow regime on the east slope of the Rockies and again produced a surface convergence zone 60 km to the lee of ridge top. Here, a weak convective element formed by 1800 MST, this time lacking the support of a strong moisture supply from the east. Recall that the substantial weakening of the convection intensity as the system moved onto the western High Plains was observed as mentioned in section 2.

By 1700 MST, the streamflow field displayed in Fig. 9 was characterized by mesoβ-scale subsidence superimposed on the primary rainshaft. Nevertheless, this region still possessed the most active updrafts because of the unique coexistence of strong CAPE and a weakened inversion. The original up-branch of the mountain plains solenoid was found propagating laterally and upwind away from the rainshaft. This breakdown process is reminiscent of the production of transients from a prescribed heat source modeled by Fulton and Schubert (1980). They demonstrated that as the transients move away upwind vertical motion redevelops, much the same as the water surface oscillates up and down in the region of impaction of some object.

This upward rebound, in fact, occurred in the simulation by 1730 MST, marking a beginning of the resurgence of strong convection in the system core. At this time, the relative surface low was reestablished in conjunction with a moderate convergent boundary-layer flow regime. A particularly strong perturbation within the precipitation field at 1715 MST produced a surface mesoγ-scale front, originating from a precipitation shaft, which forced a strong updraft within the mesoβ-scale convergent flow. By 1730 MST, peak vertical motion strengthened again to 15 m s^{-1}. This marked the beginning of the fourth stage of development.

During the period between 1700 and 2000 MST, the simulated convective system moved from the Limon, Colorado, area eastward to the Colorado and Kansas border. Over the course of this progression, peak updrafts remained between 4 and 28 m s^{-1}, as the strength of individual convective elements and the mesoscale response varied. The mesoβ-scale up-branch grew in intensity until 1800 MST, then weakened until 1900 MST, and finally strengthened dramatically until 2000 MST.

Figure 9 also depicts the streamflow evolution through this period. It is particularly interesting that the intensity of the mountain–plains solenoid grew strongly between 1900 and 2000 MST, where very high intensity was achieved. The peak intensity at 2000 MST seems to occur when, for a brief moment, all of the mesoscale convergence was concentrated into the support of a single convective element. At this time, the mesoscale convergence was also especially intense.

The structure of the mature system at 2000 MST is displayed in Fig. 11. Note the strong temperature signature at upper-levels, which was most apparent at 2000 MST. Deep warming was found on the western side of the core and shallow warming extended from the core eastward into the anvil. Strongest warming (2 K) was found near 8 km MSL in the region of the core. These features seemed to match closely the composited vertical motion and temperature profiles for MCCs obtained by Maddox (1983) and Lin (1986).

Surface moisture east of the mesoβ-scale system core continued to be capped by the plains inversion, as was evidenced in the θ_e and r_v fields. This feature was strikingly persistent and suggested that the inversion was central to focusing the system-induced heating. In fact, in early aborted attempts to perform this simulation, use of a drier soil caused excessive heating over the plains, which washed out the inversion. The result was that convection, much weaker due to lack of moisture, failed to organize a dominant single meso-β core. This suggests that the plains inversion may be one of the most essential ingredients to the mesoscale organization process. The importance of a capping inversion to focusing convection has been recognized by a number of investigators (Varney 1926; Humphreys 1926; Beebe

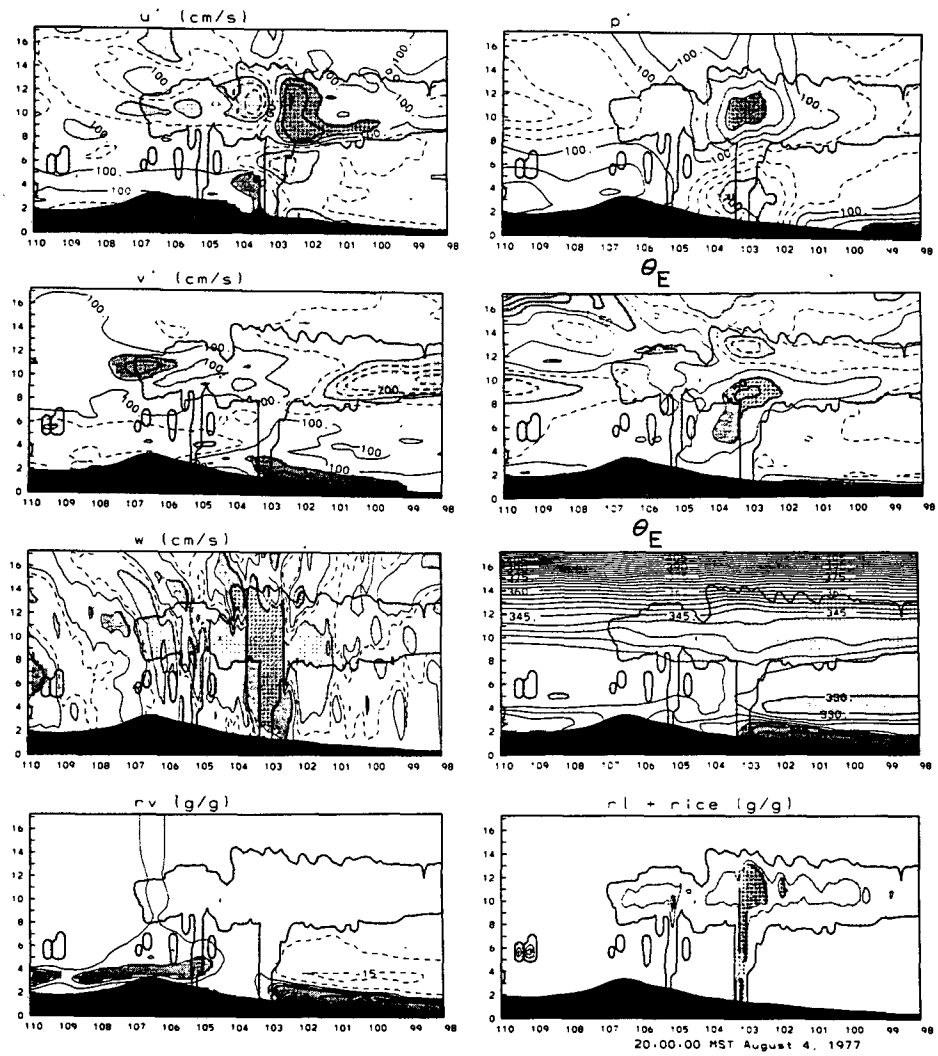

FIG. 11. As in Fig. 6, except for 2000 MST, v' contours are 2 m s^{-1} with heavy/medium shading emphasis at ±0.7 mb.

and Bates 1955; Maddox et al. 1977; Caracena and Fritsch 1983).

The upward propagation of gravity–inertia wave energy from the system core is apparent from the wave fronts radiating from the system core, which tilt eastward and westward with height in the stratosphere. Note also the weak reflection of these waves, as evidenced in the low-level vertical motion fields east and west of the rainshaft, suggesting a substantial loss of energy to the stratosphere. The vertical motion regimes 200 km (2.5° longitude) east and west of the system core are what is left from the first major growth regime, which broke into transients at 1630 MST.

A weak rainshaft over the original mountain-wave convergence zone was simulated at 2000 MST. Convection in that region was triggered by vertical motion induced by the transient gravity-waves that are still apparent. There is some evidence of this in the observations as well (see Fig. 23, GCWM). It is important to realize that the transients failed to trigger convection alone, but did so when it encountered other, more persistent, support by a deep mesoscale circulation. On the other hand, the mesoscale circulation also failed to initiate convection until it received deep vertical motion support from the transient waves. Because of previous local stabilization, the convection in this region was of only minor intensity and dissipated later as the transient internal gravity-wave moved through.

It is also interesting to study the meridional velocity field. Because this is a two-dimensional simulation, the v field represents the geostrophic part of the wind and the u field is the divergent part. It is significant that a substantial anticyclonic outflow had formed at 20 kPa and a strong cyclonic circulation was found at lower levels. These circulations were partially supported by a strong mesoα-scale low pressure near the surface and a mesoα-scale high pressure aloft. It is consistent with the known Rossby radius of 300 km (based on the simulated gravity-wave movement of 30 m s^{-1}) that the meridional circulation is on a scale of 600 km, which is far beyond the mesoβ-scale of the convective core. The dynamics and thermodynamics of this system are addressed in detail in Part 2 of this paper.

The u-component reversed from surface easterly flow west of the primary rainshaft at 102.5°W to westerly flow east of that point. It is perhaps significant that this westerly flow reaches only about 5 m s^{-1}, which is much slower than the system propagation speed. Recall that weak westerly flow of this order was found in the observations behind the convective line as it moved through eastern Colorado.

Observational evidence for the anticyclone aloft can be found in the wind field depicted by CGWM in their Fig. 28. The cyclonic circulation is also observed at low-levels; however, the low pressure is less evident in surface observations. It seems that this inconsistency may be attributed primarily to the influence of the shallow, cool airmass, which invaded from the north, and partially to biases arising from the reduction of pressure to sea level.

The anvil depicted at 2000 MST was simulated to be somewhat larger than was observed by satellite. This is primarily due to the existence of too many very small crystals resulting from inadequacies of the microphysical parameterization and perhaps by an enhanced divergence in the two-dimensional framework. Although the actual water content of the extended anvil was very small (being on the order of only 0.1 g kg^{-1} at the western boundary), its impact could be significant because of its effect on the radiation budget.

After 2000 MST, the mesoscale organization persisted, but the conditional instability weakened as nocturnal cooling set in. The dynamical structure of the system then changed significantly as a result. Following the explosive growth just before sunset, the solenoid weakened and experienced another major breakdown by 2100 MST. Unlike the first major mesoβ-scale breakdown in the suppression zone to the lee of the foothills, each successive breakdown failed to completely reverse the upward vertical motion at the core. This was indicative of a greater mesoα-scale contribution to the solenoid than earlier.

The increase in mesoα-scale circulation intensity can be seen by noting the increase in outflow momentum at 250 km east of the up-branch between 1400 and 2000 MST in Fig. 9. This can be seen to increase from three to six streamlines, or nearly 100%. The effect of scale on the behavior of the transients will be discussed to a greater extent later and evaluated more quantitatively in Part 2 of this paper.

An important change in the storm's behavior took place after 2000 MST. Unlike before sunset, the mesoβ-scale gravity-waves emitted from the core during previous circulation breakdowns began losing very little amplitude as they moved laterally beneath the anvil. They behaved as if they were suddenly trapped beneath the anvil. In fact, much stronger propagation into the stratosphere was apparent for wave energy moving beyond the anvil to the west. At 2300 MST, the amplitude of upward motion near the eastern domain boundary exceeds 20 cm s^{-1}, whereas earlier it failed to exceed the shading threshold at that distance from the emitting source. As a result, the mesoα-scale vertical motion became redistributed over three (at this time) mesoβ-scale up-branches, with each individual branch having less intensity than the parent up-branch. This weakened the primary branch, while the other branches still did not initiate convection. This important feature is discussed more fully in Part 2 and is shown to be a probable wave-ducting phenomena resulting from radiatively induced destabilization of the leading stratiform region after sunset.

The dominant horizontal wavelength of the mesoβ-scale gravity–inertia waves was about 160–240 km.

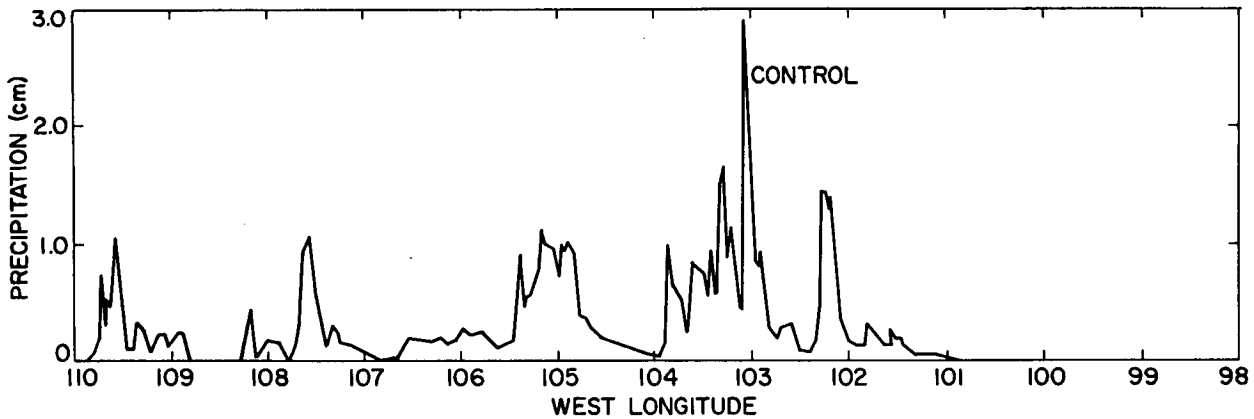

FIG. 12. Accumulated precipitation in cm versus horizontal location west longitude.

Using the 2000 MST positioning as a guide, the wave was traced to move at 21 m s^{-1} to the west and 41 m s^{-1} toward the east. Since the mean wind speed was about 10 m s^{-1}, this corresponds to a 30 m s^{-1} relative phase speed. The Brunt–Väisälä frequency of the troposphere is about 0.015 s^{-1} and the wave depth is about 12 km. This would give an internal wave speed of about 28 m s^{-1}, close to the simulated movement.

The oscillation of system intensity due to the periodic emission of transients is evident in the accumulated precipitation field shown in Fig. 12. Note the steady increase in precipitation from the ridge top genesis zone until the longitude of 105°W is reached. The suppression of precipitation was strongest at 104°W. Afterward (eastward) precipitation recovered but underwent a continuing oscillation in intensity as it moved eastward. A large component of this oscillation is on the 86 km scale, 1° longitude, which is slightly less than a 2 hour period for a system propagation of 10 m s^{-1}. It should not be surprising that this is the time scale of the mesoβ-scale transients, which are apparently controlling the intensity of mesoγ-scale convection.

Some oscillation on a 0.25° longitude or 0.5 hour time scale is also apparent, representing the lifetime of the mesoγ-scale component. Note that east of 102°W (the eastern Colorado border) the precipitation drops dramatically. This was a consequence of the system weakening as low-level, lower-valued θ_e air was injested into the system core.

As shown in Fig. 13, the simulated peak vertical motion weakened dramatically by 2330 MST, marking the dissipating stage. The dissipating stages were typified by a basic change in the structure. As the surface cooled, the thermal mesoscale support for the easterly slope flow waned. The impact was that the mesoscale dynamics were no longer capable of lifting surface air to free convection at 0200 MST.

The mesoα-scale signature in the meridional velocity, pressure and temperature fields persisted as the mesoβ-scale component weakened. As the system decoupled from the cooling surface, the surface mesoα-scale low pressure lifted to 3–5 km AGL. With it, the primary horizontal convergence moved also. Overall, this decoupling was similar to that observed by Cotton and others (personal communication) during the recent AIMCS (Airborne Investigations of Mesoscale Convective Systems) and PRE-STORM experiments, in almost all cases as the systems approached midnight.

The observed system grew larger at this time and finally reached MCC status (see CGWM). The difference between observations and the simulations can readily be attributed to the following: the observed system was some 60–80 km east of the simulated location at the critical decoupling time. This was a location where the reference flow became especially invalid. In fact, a strong, low-level mean zonal pressure gradient was observed on the western boundary of the subtropical high. As a result, a nocturnal southerly jet developed in response to geostrophic adjustment from the daytime circulation (McNider and Pielke 1981). As explained in section 1, the low-level southerly jet transports large amounts of moisture into low levels from the south during the night. As the simulated system decoupled from the surface, it injested air strongly from the observed vertical levels of the low-level jet. If this jet structure were simulated, it is possible that the simulated system would actually have reacted as observed, instead of dissipating. As it stands, it has been shown that the action of the mountain valley circulation in a basic horizontally homogeneous zonal flow will, in itself, deliver a suitable trigger to the region of the nocturnal southerly jet The simulation of the interaction of this trigger with the jet is a topic for further study.

The structure of the simulated system, however, as it passed into central Kansas resembles the structure of a mature MCC. The Rocky Mountain slope flow system, in the absence of synoptic effects, has delivered to central Kansas by 0200 MST a warm-core, partially

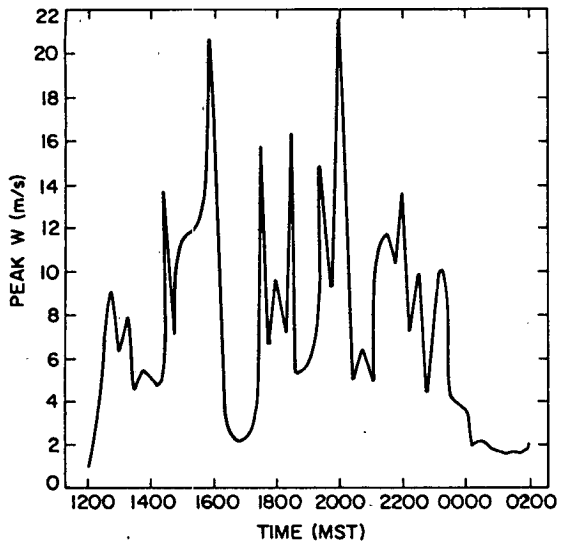

FIG. 13. Peak vertical motion (associated with system core convection) versus time.

geostrophically balanced wind system with cyclonically sheared winds of 2–4 m s^{-1} at low-levels and anticyclonically sheared winds of 6–8 m s^{-1} at upper-levels. The leading mesoβ-scale transients were quite interesting, since they closely parallel the development scenario described by McAnelly and Cotton (1986), where mesoβ-scale convection appeared ahead of the primary mesoβ-scale system core shortly after sunset.

In the next section, the evolution of the cloud field during the mature phase is discussed. This will more clearly place the mesoβ-scale evolution of transients into perspective.

d. Mesoγ-scale evolution

In order to gain insight into the nature of the individual convective elements comprising the primary convective system, a close-up of the evolution of the main precipitation shaft during Stage 5 is displayed in Fig. 14. This figure depicts grid-scale eddies that are essentially filtered out in previous figures. Here the entire displayed domain is only 100 km across, rather than 1000 km as before. The fields of w and dw/dt are displayed, where

$$\frac{dw}{dt} = -\theta_o \frac{\partial \pi}{\partial x} + \left(\frac{\theta'}{\theta_o} + 1.61 r_v - r_T\right) \qquad (6)$$

and where π is the exner function, θ_o the base state potential temperature, r_v is the vapor mixing ratio, and r_T the mixing ratio of total water. The value of dw/dt is then the current Lagrangian acceleration of w by the hydrostatic imbalance. Note that the convection is comprised of several elements. Together with w, the tendency of vertical motion is displayed.

All of the individual convective elements are contained within the general precipitation shaft. Most evident is the degree to which the mesoγ-scale growth and breakdown process parallels the mesoβ-scale activity. By comparing the dw/dt term to w, there seems to be some tendency for the upward acceleration centers to exist to the right of the upward motion patterns on the right (eastern) side of the core and to the left of the upward motion patterns on the left (western) side of the core. This suggests that the mesoγ-scale motion field is driven by propagating gravity-waves emitted near the center of the mesoβ-scale updraft, perhaps by the breakdown of a major convective element there. The dominant wavelength seems to be on the order of 20 km in the horizontal. Propagation into the stratosphere is less apparent than on the mesoβ-scale and seems to be strongest as the wave strength increases toward 2000 MST.

Recall that the period illustrated in this figure represents one of explosive mesoβ-scale growth. This seems to be manifested on the mesoγ-scale by the emergence of a single dominant mesoγ-scale wave mode. The existence of other wave modes persists but is masked by the overwhelming influence of the growth at the centroid. At any given instant, there appears to be about four to six significant waves of mesoγ-scale activity. The total combined scale of the mesoβ-scale activity then is about 100 km which reflects the scale of the upbranch of the 150–200 km, mesoβ-scale wave.

The time period of the mesoγ-scale wave is on the order of 30 minutes or that of a cumulonimbus lifetime. This is likely no coincidence and may suggest that deep convection is highly modulated by the wave train it forces (i.e., wave-CISK). The influence of seemingly nonlinear mesoβ- and mesoγ-scale interaction, however is strikingly apparent and demonstrates the complexity of the system.

Because the streamflow analysis displayed above represents only the mesoβ-scale flows, it is interesting to consider the trajectories followed by individual parcels. These trajectories take into account the evolving flow field and the mesoγ-scale variation. In order to obtain such trajectories, the local model flow fields, saved on tape, are interpolated in time and a forward–backward trajectory model is applied to parcels initialized at selected positions. The start-up positions are obtained by selecting parcels across the updraft core and within the subsidence regions at 2000 MST. The trajectory model is then run both forward (to see where the parcel goes) and backward (to see where the parcel originates).

Selected updraft and downdraft trajectories are displayed in Fig. 15. Like the streamline calculations, the storm movement of 10 m s^{-1} has been removed from the trajectories. It is interesting that the downdraft (or

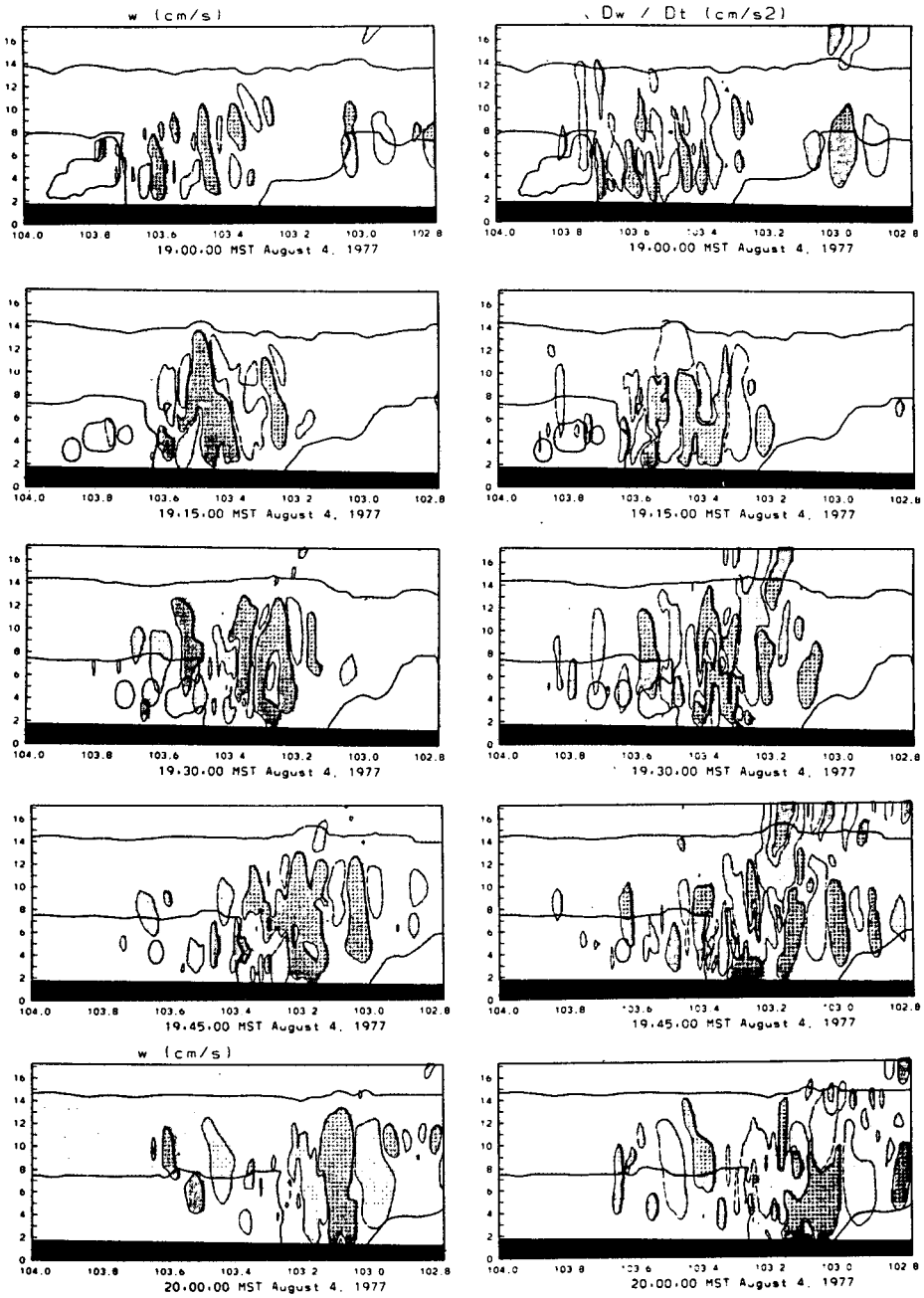

FIG. 14. Predicted mesoγ-scale fields at 1900–2000 MST. Variables displayed are w and dw/dt. Heavy (medium) shading depicts regions of motion greater (less) than $2(-2)$ m s^{-1}. Cloud outline, axis and topography are represented as in Fig. 5. The vertical coordinate is exaggerated by a factor of 4.

subsidence) forms to the west of the MCS core. The subsidence trajectories seem to be overtaken by the MCS from the front and exit the rear.

The updraft trajectories were much easier to find. There seems to be three types. The primary updraft trajectories approach from the east at low-levels and exit toward the east at upper-levels. It can be seen that at least one of those trajectories was drawn upward prior to actually entering a convective updraft. The second type of updraft is similar to Knupp's (1987) "up–down" downdraft component, but in this case the trajectory fails to subside to its original inflow-level. This is because it is warmer than the air to the storm rear which originates at colder θ_e levels.

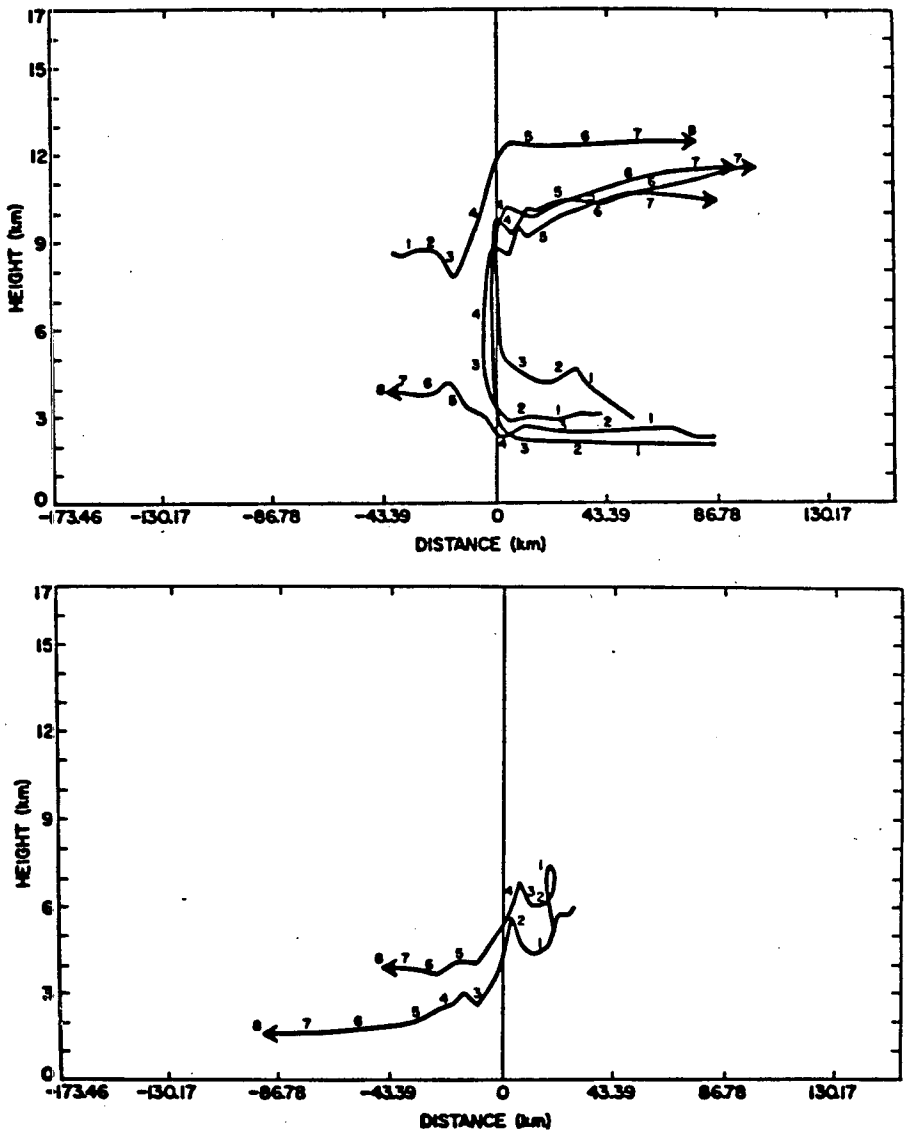

FIG. 15. Parcel trajectory paths relative to the system core. The system core is represented by the vertical line in the center of the plot. The horizontal axis is distance from the core center and the vertical axis is height above MSL in 10^3 m. The numbered positions along the trajectories represent positions on consecutive 15 min intervals. Position 4 is at 2000 MST.

The third type of updraft is associated with strong jet-level flow that overtakes the storm and flows over the top. This is somewhat a two-dimensional effect and would likely be less in three dimensions by flow around towers.

Generally, the trajectory flow agrees with the streamflow pattern except for the following. The parcel trajectories indicate cross-stream line (and even cross-trajectory) flow at the base of the storm. This suggests a turbulent exchange of mass from the moisture-rich boundary-layer to the up-branch of the streamflow and a reverse exchange for the downdraft and horizontally constant streamflow near the surface. This is not surprising and is certainly important in order to account for the high-valued θ_e air of the up-branch and cool surface air to the west. It is significant that the cool surface outflow is derived primarily from air parcels ahead of the system. This is contrary to some midlatitude MCS models but is consistent with this case where relative flow to the rear only occurs at high levels. Because the air behind the system has been modified by the convection and has been moistened at midlevels, it is especially difficult for it to support a downdraft. The low-level structure resembles the tropical squall

structure described by Moncrieff and Miller (1976), Gamache and Houze (1982) and others, in that both the updraft and downdraft air approach the system from the front. Unlike the tropical case, however, the system moves with a midlevel steering wind rather than propagating faster than all tropospheric winds. As a result, the anvil extends ahead of the system rather than behind as in a tropical structure.

5. Conceptual model of the governing dynamics

We now propose a conceptual model of the orogenic MCS structure and development process. Many of the insights of this model have been gained through additional analysis reported in Part 2 of this paper.

It is apparent from these results that no one dynamical structure persisted throughout the entire life cycle of the mesoscale system. Instead, the controlling dynamics evolved from an initial externally driven shallow solenoid to a self-maintained, deep semigeostrophic mesoα-scale convective system. We therefore divide the dynamical regimes into six distinctive stages as follows:

a. Stage 1: Dry solenoid

During the morning hours, the mountain–plains slope flow forms. On the eastern slope, a shallow solenoid develops with the easterly flow below the nocturnal inversion and the westerly flow above. The flow is driven by a zonal baroclinicity formed by the elevated mountain heat source. This leads to the acceleration of a shallow solenoid (3–5 km AGL) on the east and west sides of the slope. At the same time, downward transport of westerly momentum on the lee side of the Continental Divide dominates the balance of forces, forcing the leeside solenoid up-branch 60 km east of the Continental Divide.

Over the horizontal scale of 600 km, the east slope solenoid acts to laterally mix potentially warmer air over the ridge with potentially cooler air over the plains. At the same time, the lingering effects of the nocturnal drainage wind confine the upslope beneath the deep plains nocturnal inversion and confine the return flow to above the inversion. The result is an adiabatic cooling of the air below the inversion and the subsidence warming of air above the inversion. In effect, the surface warming is transferred to the atmosphere above the inversion without the coincident movement of moisture. This acts to maintain an inversion around 1 km AGL over the plains, capping the moisture-rich air over the plains.

Because of the regional scale of the circulation, geostrophic adjustment to the slope flow takes place. As a result of the long time scale of geostrophic adjustment (18 hours is the one-half pendulum day), a residual anticyclonic meridional flow about the Continental Divide formed by nocturnal drainage flow actually adds to the rate of the morning slope flow development. Therefore, during Stage 1, the mountain–valley circulation of the Rocky Mountains acts to induce a shallow mesoα-scale horizontal circulation in concert with the mass field to which the solenoid flow is responding. At this time, the developing circulation is in no way connected with mountain cumulus convection.

Also during Stage 1, the first mountain cumulus clouds appear. On a much smaller scale than the general mountain–plains circulation, local mountain peaks induce very shallow slope flows within the general mountain–plains solenoid that lead to the formation of some cumulus clouds over mountain peaks. Over the region of South Park, Banta (1986) found that momentum mixing induced by these local flows can lead to propagating shallow surface convergences between the free air momentum aloft and the local slope flow at the surface. The shallow convection presumably is controlled by these convergences, which move with momentum entrained from aloft. At this time, all convection is entirely dependent on these local convergences. The mountain-wave and solenoid convergence zone remains stationary at this time, its position determined by the competition between baroclinically induced zonal wind acceleration and vertical momentum transport (see Part 2). During this time, locally forced shallow convection is confined to the region west of and over the mountain convergence zone since the plains inversion acts to cap the boundary to the east. Given more westerly synoptic-scale flow at low levels, it is plausible that this convergence zone could be severely weakened or eliminated. This is a topic for further study.

b. Stage 2: Deep convection

During this stage, deep cumulus convection first appears over the upper mountains as the first low-level moisture is carried into the area by the developing valley breeze. This forms the first deep convection over the Continental Divide in association with west slope moisture. A conceptual model of this stage is given by Fig. 16. Observations indicate that on days where west slope moisture is unavailable, east slope moisture will not lead to strong convection in the South Park region until late afternoon. Such a delay in development would not place the orogenic system out on the plains until late in the day in an environment of increasing convective stability. Hence, it is suggested that western slope moisture is an important ingredient to orogenic development. A second region of convection forms 60 km east of the Continental Divide in association with strong dynamical support arising from a convergence between mountain-wave flow and developing slope flow. The exact positioning of this convergence zone relative to the ridge top varies with the intensity of the mean wind and therefore represents a competition be-

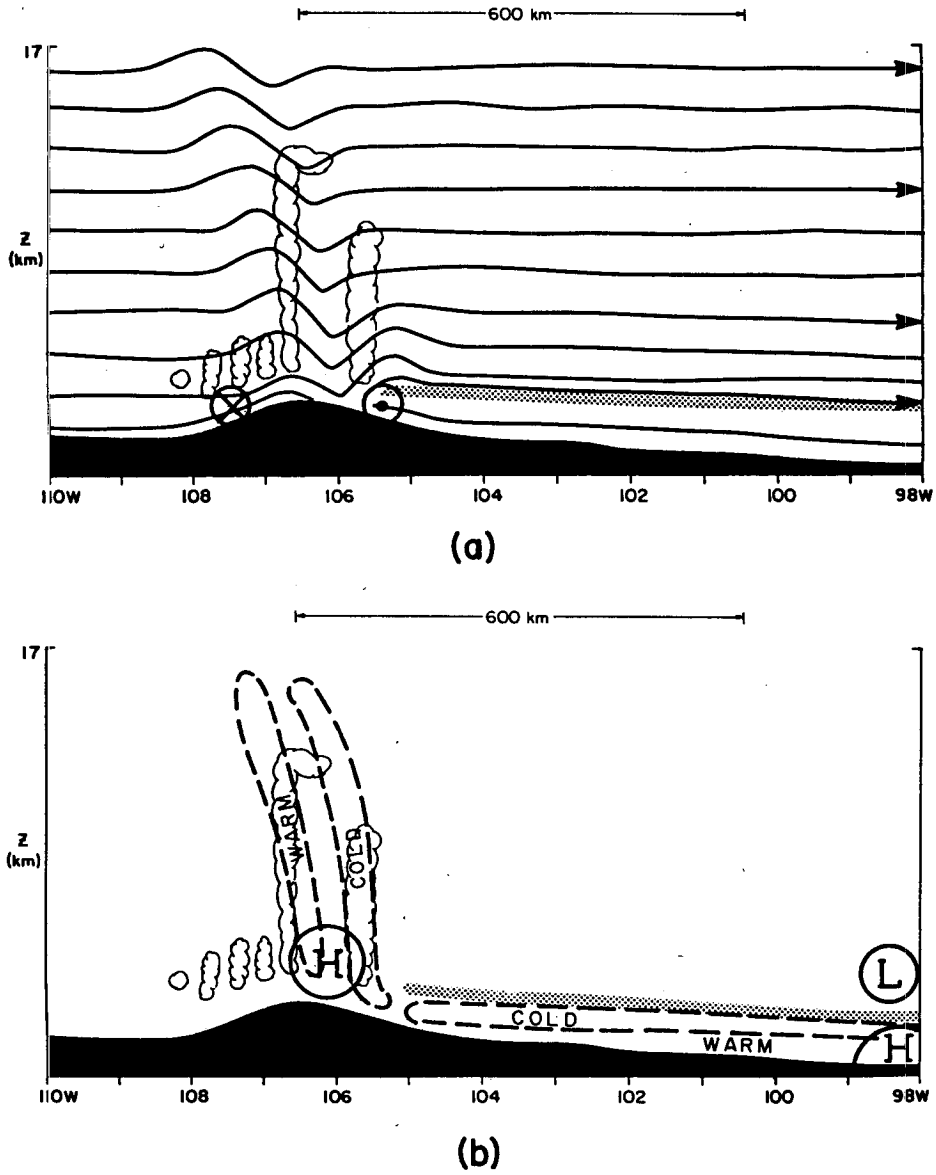

FIG. 16. Stage 2. Conceptual model showing flow field and position of convective elements at the time when deep convection forms. Axes and topography are as in Fig. 4. The stippled line represents the position of the plains inversion. Regions of cloud are indicated. Part (a) depicts the flow field with ground-relative mesoβ-scale streamlines. Circles depict flow perturbation normal to plane. Part (b) depicts the pressure and temperature response. Pressure centers are depicted by solid closed contours and temperature by dashed contours. The length scale of 600 km ($2L_R$) is indicated.

tween thermal upslope flow and downward momentum transport by the mountain-wave regime. Because the slope flow along the eastern slopes must operate in opposition to the mean lower-tropospheric flow, the transport of moisture-rich eastern plains air to the mountain-wave convergence zone is weaker than moisture transport along the western slope.

Despite the stronger CAPE supply from the west during this stage, South Park convection tends to be somewhat suppressed by leeside subsidence as towers drift eastward over the Park. At this time, the mesoα-scale mountain–plains circulation is still dominated by the baroclinicity formed by surface heating and hence remains substantially independent of the ensuing convection.

c. *Stage 3: Linkage*

Stage 3 marks the real beginning of the MCS. Prior to this time, convective elements were initiated by local

flow regimes, after which the new towers simply were shed from the source convergence and drifted eastward. Stage 3, depicted in Fig. 17, begins when the first major deep convection associated with the west slope moisture reaches the mountain–plains solenoid up-branch at the mountain-wave convergence zone. Along with the convection, a strong pulse of low-level moisture moves from the west. When the convergence zone is reached, explosive growth of convection takes place. Extensive heating results at 350 mb and the resulting induced horizontal baroclinicity overwhelms the surface heating-induced baroclinicity driving the existing mountain–plains solenoid. The result is that the convection takes control of the up-branch, deepens it to the tropopause and allows it to begin drifting eastward with the mean tropospheric wind.

d. Stage 4: The mesoβ-scale breakdown phase

A massive breakdown of the convective system is triggered by local flow anomalies existing just east of the plains and foothills boundary and marks Stage 4 in the orogenic development process. It is depicted in Fig. 18. Their effect is to weaken surface convergence into the system up-branch, forcing air to be drawn from

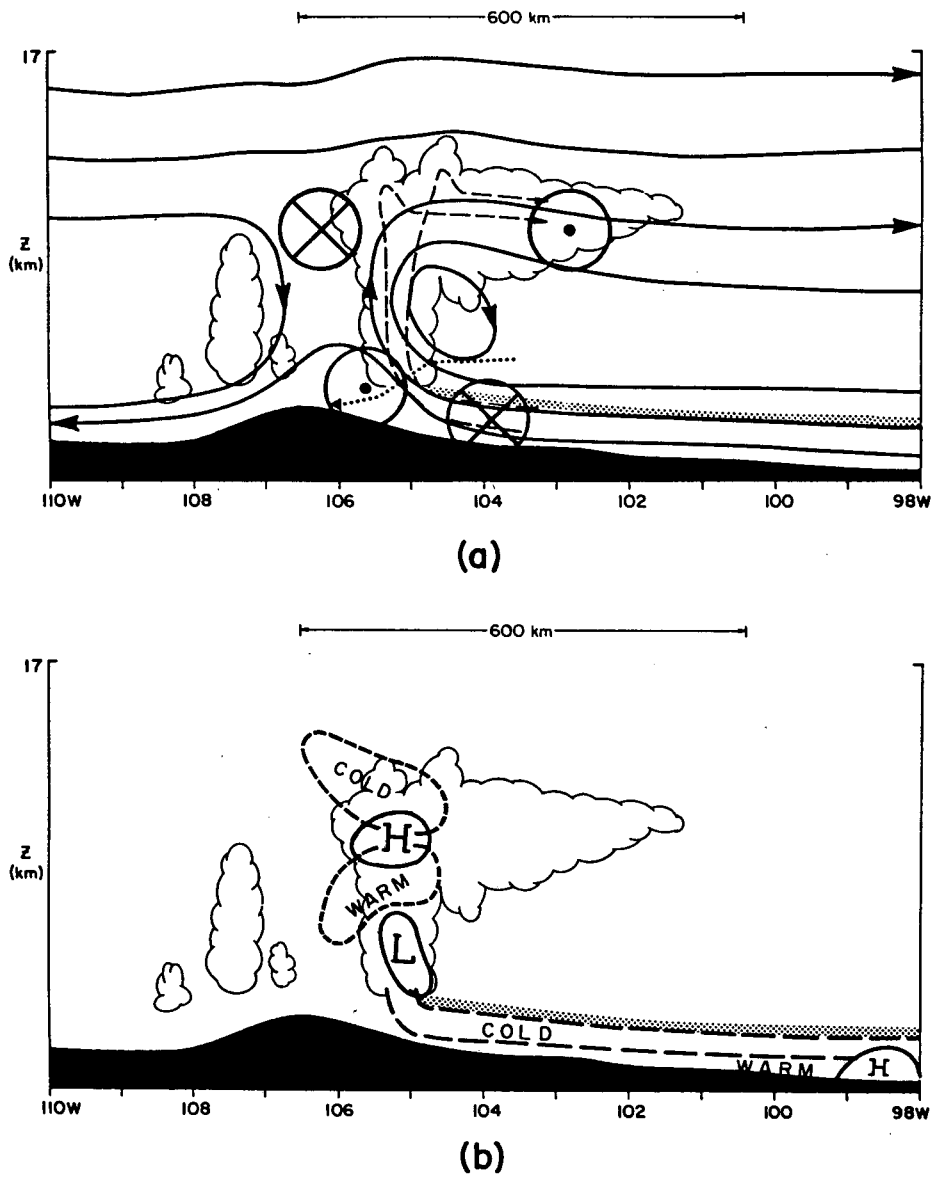

FIG. 17. As in Fig. 16, except for Stage 3. Flow is storm-relative. Individual mesoγ-scale parcel paths are given by dashed (updraft) and dotted (downdraft) lines.

lower θ_e air just above the boundary layer. This causes the system core to cool while the regions of surrounding subsidence continue to warm. The point is then reached where the core is cooler than the surrounding subsidence regions. This results in the local reversal of mesoβ-scale horizontal pressure gradient and the formation of two oppositely propagating gravity-wave circulations. Convection does not remain linked to these transients. As discussed more fully below, this occurs because of airmass stabilization behind the system (to the west) and capping of surface moisture to the east. Incredibly, the up-branch convection survives the breakdown phase, and eventually, the mesoβ-scale upward motion is reestablished as the up-branch rebounds.

During the mesoβ-scale breakdown phase, mesoα-scale supported vertical motion can be expected to persist because it would be partially in geostrophic balance and have inertial stability caused by rotation. Thus the mesoα-scale motions persist on a longer time scale and help to increasingly lessen the impact of the mesoβ-scale breakdown phases as the mesoα-scale circulation increases. The mesoα-scale circulation grows over time from the effects of the pulsing mesoβ-scale circulation; its origins are discussed more fully in Part 2. Because Stage 4 is the first mesoβ-scale breakdown phase fol-

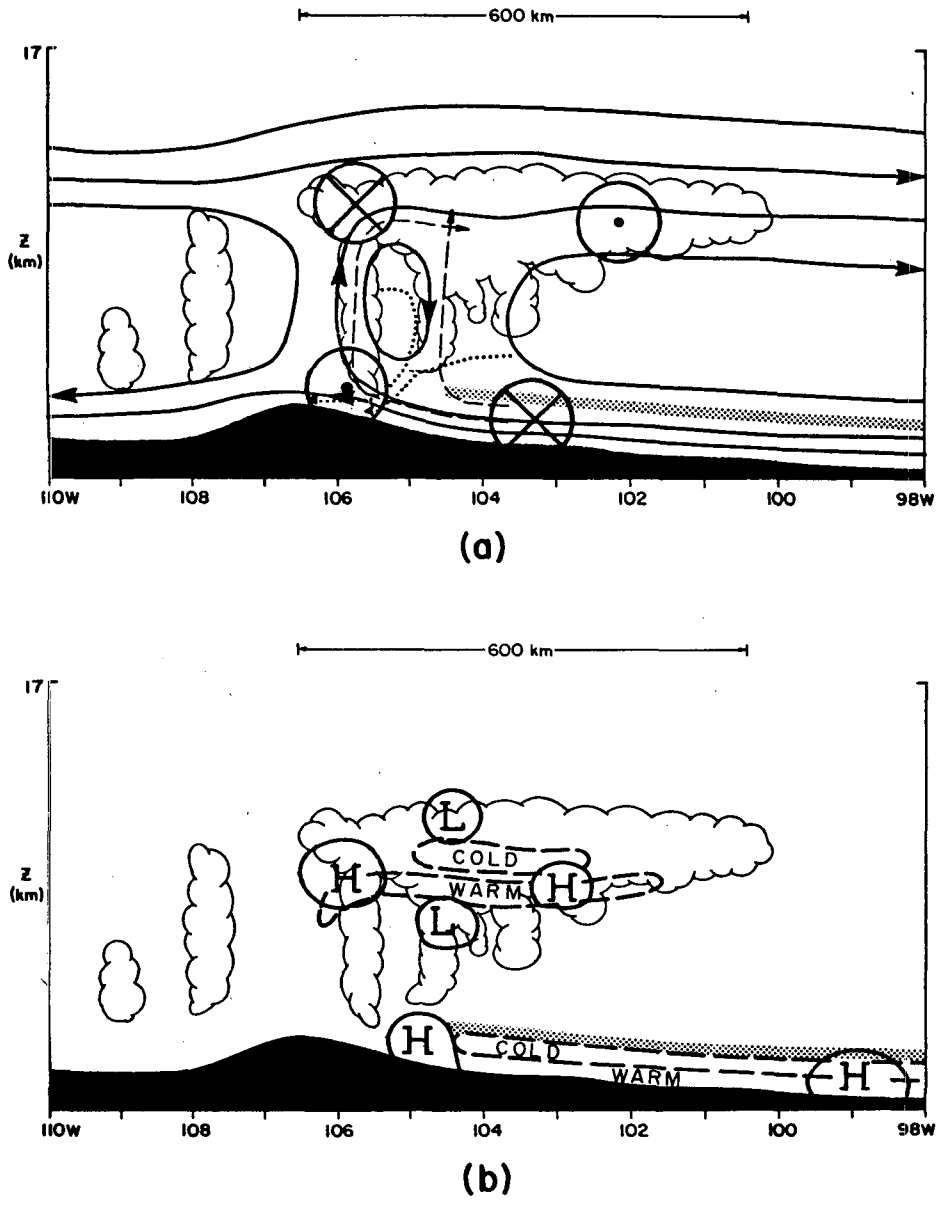

FIG. 18. As in Fig. 17, except for Stage 4.

lowing only about two hours of development, the mesoα-scale signature is weak and mean vertical motion in the vicinity of the convective core actually reverses to mesoβ-scale subsidence.

The collapse was apparently triggered at this point by the strong change in topographical slope going from the Rockies to the plains. As Dirks (1969) pointed out, this tends to produce a two-celled dry solenoid with a down-branch on the western High Plains resulting from the induced divergence of slope flow. At the same time, the early morning clear air mountain-wave pattern supported the Dirks et al. (1967) hypothesis that the western High Plains is also a region of mountain-wave-induced subsidence, which may have also contributed to the collapse of the up-branch at this location. Tripoli (1986) also simulated the mesoβ-scale flow fields of this case in a three-dimensional framework where differing eastern slopes of the Platte Valley and Palmer Lake Divide were simultaneously depicted. He found that in the Platte Valley, the change of slope is much greater moving from the foothills to the plains, and the suppression effect is far greater, causing the complete demise of convection moving off the foothills. These results suggest that this effect may be at least as important as the hypothesized convergence driven by meridional flow on the elevated east–west High Plains ridges and on the climatological favoring of convective activity over the Palmer Lake Divide. The collapse leads to the formation of east- and west-propagating gravity-waves and momentarily produces subsidence in the original region of convection. This subsidence removes the dynamical support of the centroid, while the thermodynamic support remains.

As the dynamic support moves as a gravity-wave laterally and upward, it fails to produce significant convection to the west because that air was stabilized by the prior passage of the system. To the east, a remarkable feature of the orogenic system was in operation. The slope flow, greatly enhanced by the convection itself, nurtures the existence of a plains inversion that caps the upslope flow. In the morning, this inversion reaches the surface and is associated with the nocturnal pooling of cool air. However, as the slope flow regime develops, the upslope flow forms near the surface and the return branch, downslope flow forms primarily above the inversion. As a result, adiabatic cooling in the upslope and warming in the return flow actually maintain this inversion throughout the day and suppress convection away from the solenoid up-branch. Thus, as the breakdown-phase occurs, the eastward-propagating vertical motion field is unable to tap the conditionally unstable air near the surface to the east. Thus, although the core convection is suppressed, it remains the only significant convection.

e. Stage 5: Growth of the mesoα-scale component

Following the initial mesoβ-scale breakdown phase, the mesoβ-scale up-branch recovers and again grows explosively. The mesoβ-scale circulation continues to break down approximately every 2 hours and produce new oppositely propagating transient gravity-wave circulations. A depiction of Stage 5 is given in Fig. 19. It is significant that the gravity-waves propagate upward as well and lose much of their amplitude rapidly as they move away from the genesis zone.

As time goes on, the deep mesoβ-scale solenoid grows in horizontal extent, becoming mesoα-scale itself. Appropriately, this mode grows geostrophically, inducing cyclonic shear at low-levels and anticyclonic shear aloft. As the up-branch becomes increasingly supported by mesoα-scale vertical motion, the mesoβ-scale core breakdown phases suppress the convective core less and less. Instead, the organization of the convection seems to be altered. At the breakdown times, the convection tends to spread over a large number of convective elements in the horizontal, perhaps over the mesoα-scale updraft, while during peak mesoβ-scale intensity, the convection becomes concentrated in a narrow band of much higher intensity.

At all times, the convection fails to move significantly east of the western edge of the plains inversion. The western edge of the plains inversion, on the other hand, moves eastward with the mean tropospheric wind. It is hypothesized that this is because the break in the inversion is generated by adiabatic cooling due to ascent in the up-branch of the mountain–plains solenoid, which is drifting with the mean wind and because of evaporative cooling of virga is advected eastward by the mean tropospheric wind. Were it not for the capping of the boundary-layer by the plains inversion, propagating transients initiated by the breakdown process would probably initiate convection over a wide area. This might destroy the overall mesoscale organization. On the other hand, it could lead to the accelerated movement of the system with the propagating waves.

During Stage 5, the mesoγ-scale convective circulations are strongly controlled by ongoing mesoβ-scale processes. Analysis suggests that during the growth stage of a mesoβ-scale up-branch, heating by mesoβ-scale processes is on the same order as that by mesoγ-scale processes. In fact, it suggests that the individual cumulonimbus updraft/downdraft circulations are far from independent of the mesoβ-scale circulations. In effect, individual cumulonimbi are to the mesoβ-scale circulation as individual convective turrets are to the cumulonimbi.

f. Stage 6: Controlling mesoα-scale circulation and trapped mesoβ-scale waves

As the sun sets, low-level CAPE lessens and increased net radiative cooling of the anvil top destabilizes the upper troposphere. This leads to two effects within one hour after sunset. First, the initial destabilization of the anvil increases the CAPE, momentarily leading to an explosive growth of the mesoβ-scale updraft. This is

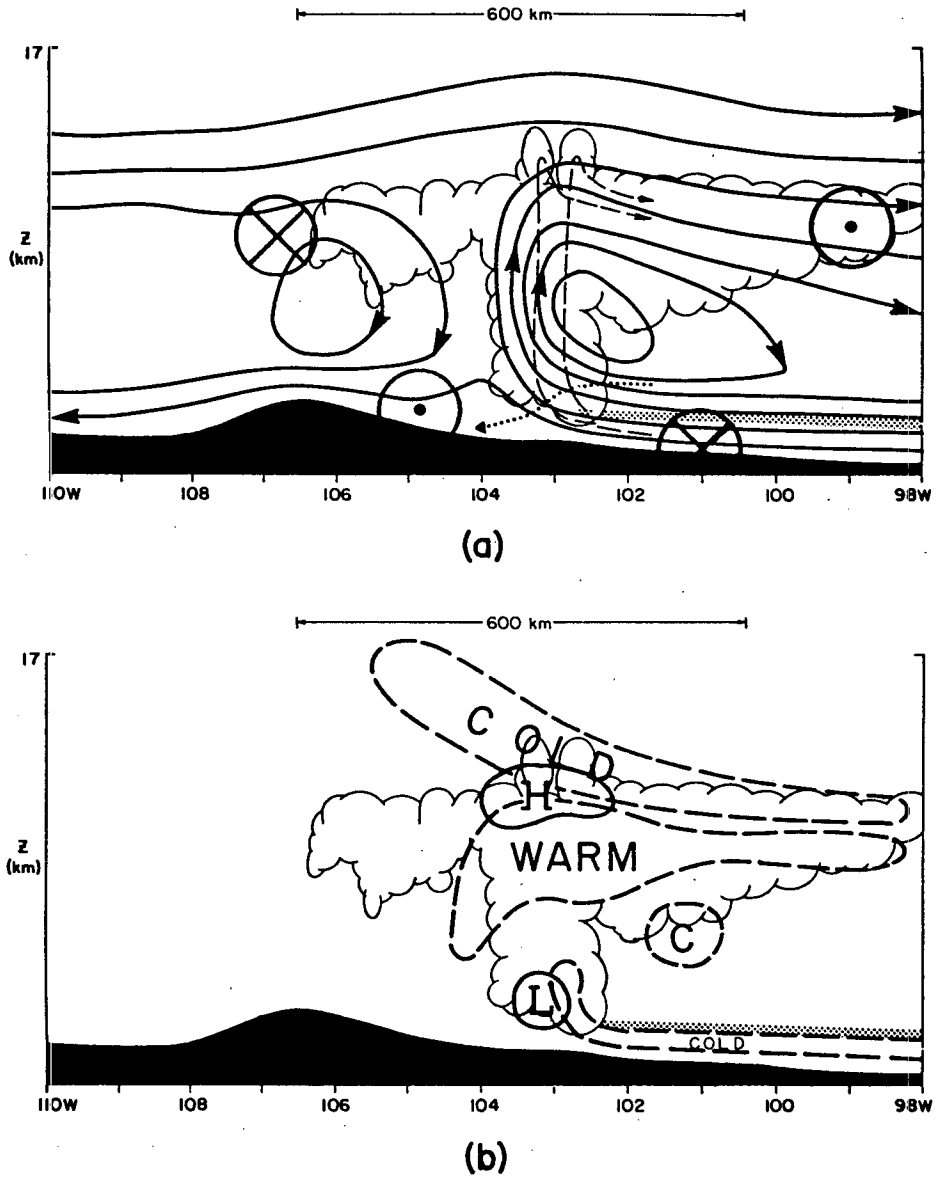

FIG. 19. As in Fig. 17, except for Stage 5.

followed by a massive mesoβ-scale breakdown process as the surface cools. At this point, Stage 6, depicted in Fig. 20, is entered.

The destabilization of the upper troposphere dramatically alters the ongoing geostrophic adjustment process by inhibiting the upward propagation of transient gravity-wave energy into the stratosphere. As the emitted transients become trapped in the troposphere and mesoγ-scale convection weakens under the diminishing surface CAPE, the formerly singular mesoβ-scale up-branch rapidly spreads over the several regions of mesoβ-scale upward motion. In three-dimensions, outward expanding rings of gravity-wave oscillations emitted by mesoβ-scale centers are envisioned intersecting with each other, producing regions of concentrated uplifting. This transformation is observed to occur on a time scale of the order of one hour with the formation of randomly organized convection beneath the stratiform anvil just after sunset The mesoβ-scale centers become relatively free of mesoγ-scale convection as the evening progresses and the tendency for the intense, small-scale circulations wanes.

It can likely be expected that the formation of more randomly distributed convection may increase the spectral projection of latent heating onto the mesoα-scale, allowing for more efficient growth of the balanced circulation. Observationally, this stage was reached as the system approached the region of the southerly jet.

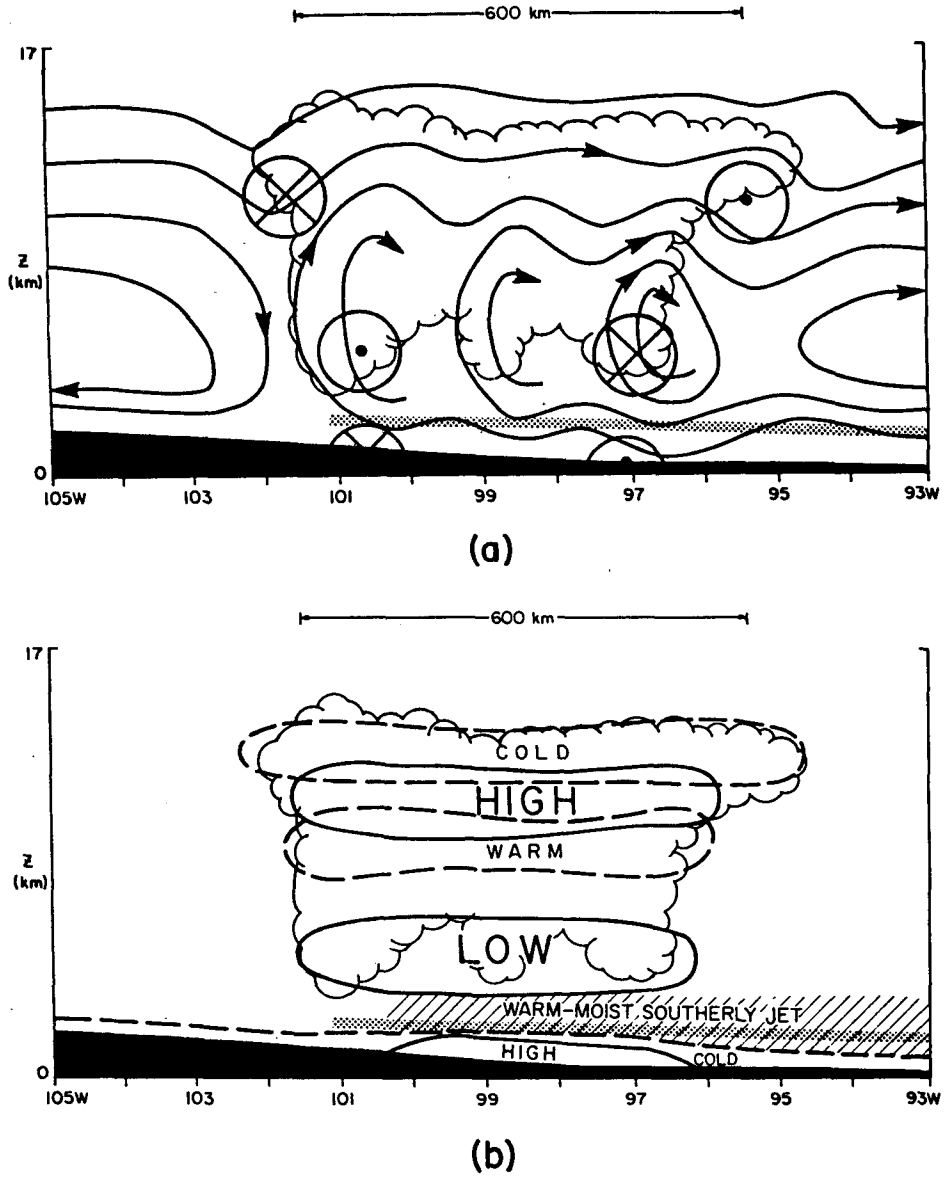

FIG. 20. As in Fig. 17, except for Stage 6. The region of the low-level southerly jet is hatched.

This provided a vigorous infusion of moisture and thermal advection at heights near the daytime inversion. Remarkably, this would feed directly into the evolving mesoβ-scale circulations in the absence of deep convection. Recall that even during the day, the mesoβ-scale circulation was coupled to inflow above the inversion, while mixing with mesoγ-scale circulations infused moisture into the core updraft.

As the above surface supply of CAPE wanes, the mesoβ-scale circulations become increasingly parasitic on the mesoα-scale upward vertical motion they produced. Recall that the mesoα-scale vertical motion was induced as a result of geostrophic adjustment to as much as 8 hours of convective heating by this time. The direct circulation of the solenoid becomes indirect as the convective support weakens and as the ageostrophic part of a semigeostrophic circulation in the form of a jet streak at upper-levels drives the vertical circulation. In the absence of a strong low-level jet (LLJ) in the two-dimensional simulation, gradual spindown of the entire mesoα-scale circulation occurs. In the simulation this occurred before midnight. If the LLJ is present, however, it is expected that the system could persist much longer or until the jet support is lost. The interaction between the evaporatively chilled mesohigh and the warm, moist LLJ provide a source of low-level baroclinicity that can sustain the deep tropospheric, solenoidal circulation.

6. Conclusions

In this paper a two-dimensional numerical cloud model was used as a tool to test the hypothesis that the observed formation of a mesoscale convective system on the western High Plains was largely self-exciting from local wind systems. The results of the simulation do indeed demonstrate that thermally driven orographic flow systems interact with ambient flow to create a favorable environment for cumulus formation and organization on the mesoscale. The fact that the development scenario closely paralleled the observed growth scenario in the absence of synoptic-scale forcing and with a grossly simplified representation of the Rocky Mountain barrier in two dimensions not only supports the original hypothesis of orogenic development, but also isolates a relatively simple mechanism of development consistent with known dynamical principals. Based on this numerical case study, a conceptual model of the orogenic development process was presented.

Perhaps the most intriguing facet of this study is that in a very basic sense, the development of the orogenic MCS is simply an ongoing geostrophic adjustment process which is highly modulated by local conditions that cause the dominant heat source to stabilize its position with respect to the mean flow. It is remarkable how the orographic flow system acts to suppress mesoγ- and mesoβ-scale convection in association with the emitted transients, causing the continuous growth of a singular mesoα-scale balanced response. Because the time scale of the geostrophic adjustment process is on the order of a half pendulum day, this latitude of 39°N can produce a significant inertial response from a diurnal flow system and in that way this phenomena may be unique to a limited region on the globe.

Some particular conclusions are listed as follows:

1) Regions of convection that eventually become the MCS have their roots in moisture advected from the west. This supports the suspected importance of the Southwest Monsoon to the episodic nature of these orogenic MCSs.

2) The importance of hot spots seems to be limited to the initial timing of the system. Without the locally forced convection, orogenic MCS development is simply delayed.

3) The initial observed mesoβ-scale explosive growth of a convective line 60 km east of the Continental Divide is forced by the interference of mountain lee wave dynamics and slope flow dynamics.

4) The plains boundary layer inversion plays a central role in the orogenic development process in two ways: 1) forming initially within the inversion of the nocturnal boundary layer, it confines early surface heating to a shallow region, inducing a strong slope flow regime and preventing near-surface moisture from mixing out into the drier air above; 2) it prevents gravity-waves emitted from the developing convective system from initiating competing convection ahead of the line, effectively focusing important convection to only the region where persistent mesoscale dynamics can erode the inversion.

5) The plains inversion itself is strengthened by the adiabatic cooling of the upslope and warming of the return flow of the slope circulation. The increase in slope flow due to the influence of convection increases the strength of the inversion, giving it the characteristic of a self-regulating phenomena.

6) The mesoβ- and mesoγ-scale components of the organized MCS undergo a continuous cycle of growth while moving with the mean wind, followed by a catastrophic breakdown phase where the energy of the developed circulation is emitted as a propagating gravity-wave. On the mesoγ-scale these waves sometimes initiate deep cumuli. On the mesoβ-scale they can induce convection west of the system where the inversion is washed out, if additional persistent mesoscale support preexists its passage.

7) Before sunset the mesoβ-scale waves lose tropospheric energy rapidly as they propagate upward into the stratosphere. After sunset, the mesoβ-scale gravity-waves become trapped beneath the anvil and persist with greater intensity in the troposphere.

8) A temporally persistent mesoα-scale component of vertical motion increases into the night. As it does, the mesoβ-scale waves act increasingly to focus mesoα-scale motion and enforce less subsidence of their own. The increased trapping of mesoβ-scale energy following sunset effectively transforms the mesoα-scale upbranch from a single intense mesoβ-scale center to several less intense mesoβ-scale centers.

It is important to recognize here that a mature MCC was never simulated. The three-dimensional structure of such systems makes that impossible to accomplish in two-dimensions. In particular, the semigeostrophic circulation, which requires thermal wind consistency for completeness, is only partially represented in the two-dimensional framework. What was accomplished with this study was to physically link several scales of transient and balanced motion in a plausible manner that attains the observed outcome of mesoscale organization. In addition, what is learned about the scale interactions can directly influence further development in the formation of mesoscale cumulus parameterization schemes.

In this paper, many of the dynamical insights described were determined by additional analysis and experimentation that is described in Part 2 of this paper. As a result, Part 2 of this paper is a more quantitative look at the governing dynamics of the MCS evolution and structure through a close examination of the physical processes acting in the model and additional sensitivity experiments. From this analysis, the conceptual model of the dynamics described here will be refined.

Acknowledgments. Thanks to Dr. Ming-Sen Lin, Mr. Ray McAnelly, Mr. Craig Tremback, Dr. Duane Stevens, Dr. Wayne Schubert and others for the many helpful discussions. Thanks also to Brenda Thompson and Lillian Vigil for typing the manuscript and to J. Michael Fritsch and A. Crook for reviewing this manuscript. This work was supported under NSF contracts ATM-8312077 and ATM-8512480. All computing was performed on the NCAR (National Center for Atmospheric Research) CRAY-1 computers. NCAR is supported by the National Science Foundation.

REFERENCES

Banta, R. M., 1986: Daytime boundary-layer evolution over mountainous terrain. Part II: Numerical studies of upslope flow duration. *Mon. Wea. Rev.*, **114**, 1112–1130.

Beebe, R. G., and F. C. Bates, 1955: A mechanism for assisting in the release of convective instability. *Mon. Wea. Rev.*, **83**, 1–10.

Bleeker, W., and M. J. Andre, 1951: On the diurnal variation of precipitation, particularly over central U. S.A., and its relation to large-scale orographic circulation systems. *Quart. J. Roy. Met. Soc.*, **77**, 260–271.

Bonner, W. D., 1963: Thunderstorms and the low-level jet. Mesometeorology Res. Pap. No. 22, University of Chicago, 21 pp.

Caracena, F., and J. M. Fritsch, 1983: Focusing mechanisms in the Texas hill country flash floods of 1978. *Mon. Wea. Rev.*, **111**, 2319–2332.

Chen, C., and W. R. Cotton, 1983: A one-dimensional simulation of the stratocumulus-capped mixed layer. *Bound.-Layer Meteor.*, **25**, 289–321.

——, and ——, 1987: The physics of the marine stratocumulus-capped mixed layer. *J. Atmos. Sci.*, **44**, 2951–2977.

Cotton, W. R., and G. J. Tripoli, 1978: Cumulus convection in Shear Flow—Three-dimensional numerical experiments. *J. Atmos. Sci.*, **35**, 1503–1521.

——, M. A. Stephens, T. Nehrkorn and G. J. Tripoli, 1982: The Colorado State University cloud/mesoscale model—1982. Part II: An ice phase parameterization. *J. Rech. Atmos.*, **16**, 295–320.

——, R. L. George, P. J. Wetzel and R. L. McAnelly, 1983: A long-lived mesoscale convective complex, Part I: The mountain generated component. *Mon. Wea. Rev.*, **111**, 1893–1918.

——, G. J. Tripoli, R. M. Rauber and E. A. Mulvihill, 1986: Numerical simulation of the effects of varying ice crystal nucleation rates and aggregation processes on orographic snowfall. *J. Climate. Appl. Meteor.*, **25**, 1658–1680.

Crow, L. W., 1969: Relationships between hail and rain in Kansas, Nebraska and eastern Colorado. LWC Rep. No. 76, Final Report, Contract No. NSF C522, National Science Foundation, 34 pp.

Culverwell, A., 1982: An analysis of moisture sources and circulation fields associated with an MCC episode. M.S. thesis, Dept. of Atmos. Sci., Colorado State University.

Dirks, R., 1969: A theoretical investigation of convective patterns in the lee of the Colorado Rockies. Atmos. Sci. Pap. No. 145, Dept. of Atmos. Sci., Colorado State University, 291 pp.

——, J. D. Mahlman and E. R. Reiter, 1967: Evidence of a mesoscale wave phenomena in the lee of the Rocky Mountains. Atmos. Sci. Pap. No. 115, Dept. of Atmos. Sci., Colorado State University, 122 pp.

Durran, D. R., and J. B. Klemp, 1982: The effects of moisture on trapped mountain lee waves. *J. Atmos. Sci.*, **39**, 2490–2506.

Dutton, J. A., and G. H. Fichtl, 1969: Approximate equations of motion for gases and liquids. *J. Atmos. Sci.*, **26**, 241–254.

Emanuel, K. A., 1983: Elementary aspects of the interaction between cumulus convection and the large-scale environment. *Mesoscale Meteorology—Theories, Observations, and Models*, D. K. Lilly and T. Gal-Chen, Eds., D. Reidel, 551–575.

Fulton, S. R., and W. H. Schubert, 1980: Geostrophic adjustment in a stratified atmosphere. Dept. of Atmos. Sci. Pap. No. 326, Colorado State University.

Gal-Chen, T., and R. C. J. Somerville, 1975a: On the use of a coordinate transformation for the solution of the Navier–Stokes equations. *J. Comput. Phys.*, **17**, 209–228.

——, and ——, 1975b: Numerical solution of the Navier–Stokes equations with topography. *J. Comput. Phys.*, **7**, 276–310.

Gamache, J. F., and R. A. Houze, Jr., 1982: Mesoscale air motions associated with a tropical squall line. *Mon. Wea. Rev.*, **110**, 118–135.

Hales, J. E., 1972: Surges of maritime tropical air northward over the Gulf of California. *Mon. Wea. Rev.*, **100**, 298–306.

Hann, J. von, 1926: *Lehrbuch der Meteorologie.* Leipzig, W. Keller, 348–453.

Henz, J., 1974: Colorado High Plains thunderstorm systems—a descriptive radar-synoptic climatology. M.S. thesis, Dept. of Atmos. Sci., Colorado State University.

Hewson, E. W., 1937: The application of wetbulb potential temperature of air mass analysis. *Quart. J. Roy. Meteor. Soc.*, **63**, 323.

Hill, G. E., 1974: Factors controlling the size and spacing of cumulus clouds as revealed by numerical experiments. *J. Atmos. Sci.*, **31**, 646–673.

Hughes, R. L., 1978: A numerical simulation of mesoscale flow over mountainous terrain. M.S. thesis, Dept. of Atmos. Sci., Colorado State University.

Humphreys, W. J., 1926: The tornado. *Mon. Wea. Rev.*, **54**, 501–503.

Kincer, J. B., 1916: Daytime and nighttime precipitation and their economic significance. *Mon. Wea. Rev.*, **44**, 628–633.

Klemp, J. B., and R. B. Wilhelmson, 1978: The simulation of three-dimensional convective storm dynamics. *J. Atmos. Sci.*, **35**, 1070–1096.

——, and D. K. Lilly, 1980: Mountain waves and momentum flux. Chap. 4, *Orographic Effects in Planetary Flows*, GARP Publ. Ser. No. 23, ICSU/WMO, 116–141. [Available from World Meteorological Organization, Case postale No. 5, CH-1211 Geneva 20, Switzerland.]

——, and D. R. Durran, 1983: An upper boundary condition permitting internal gravity-wave radiation in numerical mesoscale models. *Mon. Wea. Rev.*, **111**, 430–444.

Klitch, M. A., J. F. Weaver, F. P. Kelly and T. H. Vonder Haar, 1985: Convective cloud climatologies constructed from satellite imagery. *Mon. Wea. Rev.*, **113**, 326–337.

Knupp, K. R., 1987: Downdrafts within high plains cumulonimbi. Part I: General kinematic structure. *J. Atmos. Sci.*, **44**, 987–1008.

Kuo, H.-C., 1983: The radiation fields in maritime stratocumulus. M.S. thesis, Dept. of Atmos. Sci., Colorado State University, 91 pp.

Lin, M., 1986: The evolution and structure of composite meso-α-scale convective complexes. Ph.D. dissertation, Dept. of Atmos. Sci., Colorado State University, 245 pp.

Lindzen, R. S., and K. K. Tung, 1976: Banded convective activity and gravity waves. *Mon. Wea. Rev.*, **104**, 1602–1617.

Louis, J. F., 1979: A parametric model of vertical eddy fluxes in the atmosphere. *Bound.-Layer Meteor.*, **17**, 187–202.

McAnelly, R. L., and W. R. Cotton, 1986: Mesoβ-scale characteristics of an episode of mesoα-scale convective complexes. *Mon. Wea. Rev.*, **114**, 1740–1770.

McCumber, M. C., and R. A. Pielke, 1981: Simulation of the effects of surface fluxes of heat and moisture in a mesoscale numerical model. 1. Soil Layer. *J. Geophys. Res.*, **86**, 9929–9938.

McNider, R. T., and R. A. Pielke, 1981: Diurnal boundary-layer development over sloping terrain. *J. Atmos. Sci.*, **38**, 2198–2212.

Maddox, R. A, 1980: Mesoscale convective complexes. *Bull. Amer. Meteor. Soc.*, **61**, 1374–1387.

——, 1981: The structure and life-cycle of midlatitude mesoscale convective complexes. Atmos. Sci. Pap. No. 336, Dept. of Atmos. Sci., Colorado State University, 311 pp.

——, 1983: Large-scale meteorological conditions associated with

midlatitude, mesoscale convective complexes. *Mon. Wea. Rev.*, **111**, 1475–1493.

——, F. Caracena, L. R. Hoxit and C. F. Chappell, 1977: Meteorological aspects of the Big Thompson flash flood of 31 July, 1976. NOAA TR ERL 388-APCL 41, 84 pp.

Means, L. L., 1944: The nocturnal maximum occurrence of thunderstorms in the midwestern states. University of Chicago Press, Misc. Rept. 16, 38 pp.

——, 1952: On thunderstorm forecasting in the central United States. *Mon. Wea. Rev.*, **80**, 165–189.

Molinari, J., and M. Dudek, 1985: Implicit versus explicit convective heating in numerical weather prediction models. *Mon. Wea. Rev.*, **114**, 1822–1831.

Moncrieff, M. W., and M. J. Miller, 1976: The dynamics and simulation of tropical cumulonimbus and squall lines. *Quart. J. Roy. Meteor. Soc.*, **102**, 373–394.

Orlanski, I., 1975: A rational subdivision of scales for atmospheric processes. *Bull. Amer. Meteor. Soc.*, **56**, 527–530.

Paegle, J., W. G. Zdunkowski and R. M. Welch, 1976: Implicit differencing of predictive equations of the planetary boundary-layer. *Mon. Wea. Rev.*, **104**, 1321–1324.

Phillip, C. B., 1979: Observation of progressive convective interactions from the Rocky Mountain slopes to the plains. Atmos. Sci. Pap. No. 316, Dept. of Atmos. Sci., Colorado State University, 100 pp.

Raymond, D. J., 1983: Wave-CISK in mass-flux form. *J. Atmos. Sci.*, **40**, 2561–2572.

Redelsperger, J. L., and G. Sommeria, 1986: Three-dimensional simulation of a convective storm: Sensitivity studies on subgrid parameterization and spatial resolution. *J. Atmos. Sci.*, **43**, 2619–2635.

Rosenthal, S. L., 1979: The sensitivity of simulated hurricane development to cumulus parameterization details. *Mon. Wea. Rev.*, **107**, 193–197.

Ross, B. B., and I. Orlanski, 1982: The evolution of an observed cold front. Part I. Numerical simulation. *J. Atmos. Sci.*, **39**, 296–327.

Schlesinger, R. E., 1984: Effects of the pressure perturbation field in numerical models of unidirectionally sheared thunderstorm convection: Two versus three dimensions. *J. Atmos. Sci.*, **41**, 1571–1587.

Tepper, M., 1952: The application of the hydraulic analogy to certain atmospheric flow problems. Res. Pap. No. 35, U. S. Weather Bureau, 50 pp.

Tremback, C. J., and R. Kessler, 1985: A surface temperature and moisture parameterization for use in mesoscale numerical models. Preprints, Seventh Conf. on Numerical Weather Prediction, Montreal, Amer. Meteor. Soc.

Tripoli, G. J., 1986: A numerical investigation of an orogenic mesoscale convective system. Atmos. Sci. Pap. No. 401, Dept. of Atmos. Sci., Colorado State University, 290 pp.

——, and W. R. Cotton, 1981: The use of ice-liquid water potential temperature as a thermodynamic variable in deep atmospheric models. *Mon. Wea. Rev.*, **109**, 1094–1102.

——, and ——, 1982: The Colorado State University three-dimensional cloud/mesoscale model—1982. Part I: General theoretical framework and sensitivity experiments. *J. Rech. Atmos.*, **16**, 185–220.

——, G. J., and ——, 1986: An intense, quasi-steady thunderstorm over mountainous terrain. Part IV: Three-dimensional numerical simulation. *J. Atmos. Sci.*, **43**, 894–912.

——, and ——, 1988: A numerical investigation of an orogenic mesoscale convective system. Part 2: Analysis of governing dynamics. *Mon. Wea. Rev.*, **116**, 301–324.

Varney, B. M.,1926: Aerological evidence as to the causes of tornadoes. *Mon. Wea. Rev.*, **54**, 163–165.

Wallace, J. M., 1975: Diurnal variations in precipitation and thunderstorm frequency over the conterminous United States. *Mon. Wea. Rev.*, **103**, 406–419.

Wetzel, P.J, 1973: Moisture sources and flow patterns during the northeast colorado hail season. M.S. thesis, Dept. of Atmos. Sci., Colorado State University.

——, W. R. Cotton and R. L. McAnelly, 1983: A long-lived mesoscale convective complex. Part II: Evolution and structure of the mature complex. *Mon. Wea. Rev.*, **111**, 1919–1937.